On the Equation of State of Metals at Low Temperatures

A Thesis

presented by

Alexander Mather Ironside, B.Sc.

to the

University of St. Andrews

in application for the Degree

of Master of Science.

DECLARATION

I hereby declare that the following Thesis is based on the results of experiments carried out by me, that the Thesis is my own composition and that it has not been previously presented for a Higher Degree.

CERTIFICATE

I certify that Alexander Mather Ironside, B.Sc., has spent not less than four terms as a research student in the Physical Laboratory of the United College of St. Salvator and St. Leonard in the University of St. Andrews, that he has fulfilled the conditions of Ordinance No. XVII of the University Court of St. Andrews and that he is qualified to submit the accompanying Thesis in application for the Degree of Master of Science.

Research Supervisor

CONTENTS

LIST OF ILLUSTRATIONS

CHAPTER 1

INTRODUCTORY REMARKS

1.1 General Introduction.

The equation of state of a regular crystalline solid can be defined as a relationship which describes its pressure as a function of volume and temperature. Most solids below their melting points are an aggregate of large numbers of small crystals or grains, the size of these crystals being mainly determined by the previous history of the sample. It is usual in theoretical discussion to consider physical relationships for an ideal crystal with a completely regular structure to simplify the discussion.

The equation of state of a large crystal may be obtained from the thermodynamic relation,

$$p = -\left.\frac{\partial F}{\partial V}\right)_T$$

where p, V, and T are the hydrostatic pressure, volume and temperature respectively. The Helmholtz free energy, F, of a crystal lattice can be found by considering the

N particles of the crystal lattice as a system of 3N loosely coupled harmonic oscillators and applying the methods of statistical mechanics. If the Helmholtz free energy and thus the equation of state be derived from the quantum theory of the thermal properties of solids, then measurement of the thermal expansion will allow an experimental verification of the theoretical predictions.(1)

The equation of state of a solid has been found to be much more difficult to formulate than that of a gas and has been the subject of much theoretical argument. Because of the difficulty of measuring thermal expansion at low temperatures, little experimental work has been done in the very low temperature region where the full effects of the quantum theory of solids become apparent. The physical behaviour of a solid at low temperatures is determined mainly by the vibrational spectrum of the constituent atoms of the crystal lattice and this spectrum is in turn determined by the interatomic forces. Thus the measurement of thermal expansion at low temperatures can give evidence about the more fundamental interatomic force law.(2)

The equation of state of a solid was first given in a useful form by Mie(3) and on the basis of his work Gruneisen developed the Mie-Gruneisen equation of state,(4) beginning from the Clausius virial law and using classical statistical

mechanics. He gave the relationship,

$$pV = -V \frac{\partial \Phi_o(V)}{\partial V} + \gamma_E E_T \qquad \ldots . 1.1$$

where Φ_o is the potential energy of a gram atom of the solid in equilibrium at p=0 and T=0, γ_E is a constant for any given substance, and E_T is the thermal energy where

$$E_T = \int_o^T C_v \, dT .$$

He also showed that

$$\frac{3\alpha}{\chi_T} = \frac{\partial P}{\partial T}\Big)_v = \frac{\gamma C_v}{V} \qquad \ldots . 1.2$$

where χ_T is the isothermal compressibility and so α, the coefficient of linear expansion, is proportional to C_v if $\gamma\chi_T/V$ is constant. The ratio χ_T/V is nearly constant as a function of T so that the equation 1.2 will be true if γ is constant. This is the statement of the law that the thermal expansion coefficient is proportional to the specific heat at constant volume, first given by Gruneisen.(5) Barron(6) points out that if Gruneisen's theory does not hold, as suggested by Bijl and Pullan,(7) then γ and γ_E are not the same and functions of V only, but are functions of both V and T defined by equations 1.1 and 1.2. Variation of either then gives a measure of the departure from Gruneisen's rule.

The equation of state can also be expressed on the basis of the Debye theory of a solid.[8] The equation is derived by thermodynamic reasoning and the formula for the specific heat derived by Debye. The equation has the same form as 1.1, with

$$\gamma_E = -\frac{d \ln \Theta}{d \ln V} \qquad \ldots . 1.3$$

where $\Theta = h\nu_m/k$ and ν_m is the limiting Debye frequency, and with the Debye expression for E_T.

Because of the disagreement among current measurements of thermal expansion[9] it was thought that it would be worthwhile to repeat measurements already performed on monatomic metals. The apparatus developed is fully described in Chapter 3 and uses the principle of measurement of the change in capacity of a parallel plate condenser caused by dilation of the specimen, first used by Prytherch[10] and developed by Bijl and Pullan.[7] The object of this thesis is to summarise the developement of the theoretical equations of state and to compare their predictions with experimental data from new measurements of thermal expansion.

An apparatus has been developed which it is hoped will be suitable for making measurements down to liquid hydrogen temperatures, and experimental measurements have been made to liquid nitrogen temperatures. The developement of this

apparatus is described and some of the results obtained are presented and compared with other experimental data.

1.2 Experimental methods for measuring thermal expansion

Various methods other than capacity change have been used in the measurement of thermal expansion and these have been described elsewhere by Pullan[11] and Stewart.[12] They are a) optical interference

b) optical lever

c) direct measurement

d) pycnometer method

e) x-ray diffraction

f) other electrical methods

There have been several recent developements in these standard methods which will be described below.

The optical lever principle was used by Huzan, Abbis and Jones[13] where expansion of the specimen relative to a control specimen causes a change in the angle between two mirrors. The angle between the mirrors was measured using a microptic collimator. The accuracy quoted is 20% for a value of α of 1×10^{-6} with a temperature change of $1^{\circ}K$ at $50^{\circ}K$.

Andres[14] has described a method which transforms length changes into changes of light intensity using a com-

bination of two closely spaced parallel grids as described by Jones,[15] with a pair of photocells to measure the light intensity passing through the grids. The system is calibrated mechanically. The detection of a relative length change of about 10^{-9}cm is claimed but only preliminary results are available.[16]

White has developed a method involving the change in capacity of a three-terminal capacitor and using a transformer bridge to measure the capacity.[17] The method gives a detection sensitivity and reproducibility of 10^{-8}cm or less and promises to improve to 10^{-9}cm or better. The bridge measurement however, requires standard capacitors which are very difficult to make to the required accuracy and stability which is about 10^{-6}pF, and the apparatus appears generally more difficult to use compared to the present apparatus described in Chapter 3. Results are available for Cu, Be and Cr.[17][18][19][20]

Dheer and Surange[21] used the change in capacity of a parallel plate condenser in the resonant circuit of an oscillator as did Bijl and Pullan[7] but measured the changes in frequency using a heterodyne beat method to compare the frequency of the oscillator associated with the expansion with the frequency of a similar fixed oscillator. The accuracy of measurement of $\Delta\ell/\ell$ is given as 0.07×10^{-6},

comparable to that obtained with interferometric methods. Suitable specimens are, however, limited to those materials which are available in fairly large pieces which can be machined to the required dimensions.

1.3 The present method of measurement.

The apparatus developed differs from that of Bijl and Pullan, and that of Dheer and Surange in that the resonant circuit whose frequency is determined by the specimen is completely enclosed in the cryostat and therefore changes in the capacity of coaxial leads and other not easily controllable effects are absent. The frequency measurement is similar in principle to that used by Dheer and Surange, being a heterodyne method, but since the resonant circuit associated with the expansion of the specimen is not part of an oscillator tank circuit, it was necessary to develop a method of measuring the resonant frequency of the resonant circuit with the required accuracy.

To do this, the resonant frequency itself was changed periodically by varying one of the components in the resonant circuit. The original design by Stewart used a ferrite cored coil whose inductance was varied by applying a a low-frequency sinusoidal magnetic field to the ferrite core. The ferrite cored coil caused the resonant circuit to have

a Q-value of 15, and this was too low to provide sufficient accuracy. To improve the sensitivity it was necessary to replace the ferrite cored coil and find some other method. An audio-frequency vibrating reed condenser, described in Chapter 3.3 was incorporated in the resonant circuit in parallel with the dilatometer capacity. For a constant frequency radio-frequency input this will produce an amplitude modulated radio-frequency voltage across the coil of the resonant circuit. The phase of the modulation relative to the phase of the driving audio-frequency voltage of the vibrating reed condenser, will change as the resonant circuit is moved through its resonant frequency. The modulated radio-frequency signal was picked up, demodulated and the resulting signal amplified and compared with the exciting audio-frequency in a phase sensitive detector. In this way the resonant frequency could be determined to within 100c/s with a carrier frequency of 5.5Mc/s. Since 100c/s change is produced by a Δl of 10^{-6}cm this corresponds to a detection sensitivity for $\Delta l/l$ of 0.5×10^{-6}. It should be possible to increase the radio-frequency to 10Mc/s with suitable modifications to the electronic circuits and to improve the determination of the resonant frequency to within 5c/s or better.

For this experimental arrangement, there are no rigid

tolerances on specimen length or thickness. The only requirement is that they be about 2cm long, although smaller samples could be used with some loss in sensitivity.

CHAPTER 2

THEORETICAL CONSIDERATIONS

This chapter will summarise the developement of the equation of state of a solid indicating the main lines of thought.

2.1 The equation of state of solids.

To obtain the equation of state of a solid, a relation is required between its pressure, volume and temperature. In this discussion the pressure will be limited to hydrostatic pressure although, unlike a fluid, a solid can support a much more complex strain than a simple change of volume. The main problem in finding the equation of state of a solid is to find an expression for the Helmholtz free energy F, of the crystal lattice by the methods of statistical mechanics. If the free energy is known as a function of T and V the equation of state follows from the thermodynamic relation,

$$p = -\frac{\partial F}{\partial V}\Big)_T \qquad \ldots . 2.1$$

To do this, consider a lattice of N points with a

particle situated at each lattice point. This system can be regarded as a mechanical system of loosely coupled oscillators. If the particles are treated as point masses the assembly can be represented as a system of 6N degrees of freedom with 3N different periodic modes of vibration with 3N different frequencies ν_j $(j = 1,2,3 \ldots 3N)$. When all the eigenfrequencies are known, the free energy can be calculated from the expression

$$F = \Phi + \sum_{j=1}^{3N} kT \ln\left[1 - \exp(-h\nu_j/kT)\right] \quad \ldots . 2.2$$

where Φ is the energy at absolute zero and is the sum of the cohesive energy and the zero point energy. Differentiation with respect to volume yields the general equation of state,

$$p = -\frac{\partial \Phi}{\partial V} + \frac{1}{V} \sum_{j=1}^{3N} \gamma_j \frac{h\nu_j}{\exp(h\nu_j/kT) - 1} \quad \ldots . 2.3$$

where $\gamma_j = -V\, d\nu_j/\nu_j\, dV.$ $\ldots . 2.4$

The determination of the exact frequency spectrum is a very difficult dynamical problem and progress can only be made by simplifying the problem.

2.2 The Einstein model of a solid and its equation of state

One of the earliest approaches was due to Einstein, who used a single frequency, assuming that all the ν_j were equal.(22)

In this case equation 2.3 becomes

$$p = -\frac{\partial \Phi}{\partial V} + \frac{\gamma_E}{V} \sum \frac{h\nu}{\exp(h\nu/kT) - 1} \qquad \ldots . 2.5$$

or $$pV = -V \frac{\partial \Phi}{\partial V} + \gamma_E E_E \qquad \ldots . 2.6$$

where E_E is the vibrational energy of the Einstein solid and where

$$\gamma_E = -\frac{d \ln \nu}{d \ln V} \qquad \ldots . 2.7$$

Equation 2.7 shows that γ_E describes the dependence of the lattice frequency on the volume. Differentiating equation 2.6 and using the relationship

$$\left.\frac{\partial p}{\partial T}\right)_V = -\left.\frac{\partial V}{\partial T}\right)_p \Big/ \left.\frac{\partial V}{\partial p}\right)_T$$

gives a relation between γ_E and the coefficient of thermal expansion

$$\gamma_E = \frac{V \alpha}{C_{VE} \chi_T} \qquad \ldots . 2.8$$

where $$C_{VE} = \left.\frac{\partial E_E}{\partial T}\right)_V \qquad \ldots . 2.9$$

and χ_T is the isothermal compressibility. Since V and χ both tend to finite constant values as T tends to zero, then if γ_E is a constant the thermal expansion coefficient will be proportional to the specific heat C_{VE}.

Einstein recognised that the vibration of a particle

at a lattice point in a real solid cannot be harmonic because of the strong influences exerted on it by neighbouring particles in the lattice.[23] He suggested that several frequencies be used since if one considers the Fourier analysis of the vibration, the motion can be characterised by the various harmonics of the Fourier series representing the motion. This led Debye to make a new approach to the problem.

2.3 The Debye model of a solid and its equation of state.[8]

Debye began from the ordinary equations of elasticity, treating the solid as a dispersionless continuum with an infinite number of eigenvibrations. He allowed for the obvious error in this by limiting the number of vibrations to $3N$. This gave a lattice-frequency spectrum which took account of the expected characteristics of a solid without considering in detail the forces between atoms. The Debye spectrum was parabolic, given by the frequency distribution

$$\rho(\nu) :: \nu^2 \qquad \left\{ \begin{matrix} 0 < \nu < \nu_m \\ \int \rho(\nu)\, d\nu = 3N \end{matrix} \right\}.$$

The Debye equation of state is then derived by expressing the free energy as

$$F = U - TS$$

and using the Debye expression for the internal energy U where

$$U = \int_0^T C_v \, dT$$

and the entropy S is given by

$$S = \int_0^T \left[C_v/T\right] dT = \frac{U}{T} + \int_0^T \left[U/T^2\right] dT$$

This gives for F, the free energy of a gram molecule at temperature T and volume V

$$F = \Phi + 3RT\left\{ -\frac{T^3}{\theta^3}\int_0^{\theta/T} \frac{\xi^3 \, d\xi}{e^{\xi} - 1} + \int_{\infty}^{\theta/T} \frac{d\xi}{e^{\xi} - 1} \right\}$$

where $\theta = h\nu_m/k$, $\xi = h\nu/kT$.

It follows from 2.1 that

$$p = -\frac{\partial \Phi}{\partial V} - 9RT \, \frac{1}{T} \, \frac{d\theta}{dV} \left(\frac{T}{\theta}\right)^4 \int_0^{\theta/T} \frac{\xi^3 \, d\xi}{e^{\xi} - 1}$$

and thus $$pV = -V \frac{\partial \Phi}{\partial V} + \gamma_D U \qquad \ldots . 2.10$$

where U is the Debye expression for the internal energy and γ_D is given by

$$\gamma_D = -\frac{d \ln \theta}{d \ln V} = -\frac{d \ln \nu_m}{d \ln V} \qquad \ldots . 2.11$$

Rewriting 2.11 as

$$\gamma_D = -\frac{V}{\theta} \frac{d\theta}{dV} = -\frac{1}{\alpha \theta} \frac{d\theta}{dT} \qquad \ldots . 2.11a$$

gives $$\alpha = -\frac{1}{\gamma_n \theta}\frac{d\theta}{dT} \qquad \ldots . 2.12$$

showing that the Debye theory gives zero thermal expansion since for a Debye solid θ is independent of T. To make use of the Debye theory for a discussion of thermal expansion one must introduce a dependence of θ on volume to allow for anharmonic effects such as thermal expansion.

Agreement between the values of C_v derived using the Einstein and Debye models is good except at very low temperatures where the Einstein model gives values which are too low. Thus the sensitivity of the thermodynamic properties to the exact shape of the frequency spectrum is not significant except at low temperatures and conversely determination of the exact frequency spectrum from measurements of specific heat is not very accurate.

2.4 The Mie-Gruneisen equation of state.[3][4]

As long as the atomic vibrations of a solid are regarded as a superposition of harmonic vibrations one cannot explain the influence of temperature on the volume: with purely harmonic vibrations the solid can be shown to have zero thermal expansion(equation 2.12 above). One of the earliest equations of state came from Mie[3] on a basis of classical statistical mechanics. One should therefore expect his equation to hold accurately only at temperatures of the order

of the Debye temperature or above. Mie's method was analogous to the van der Waals treatment of liquids and considered isotropic monatomic substances under hydrostatic pressure, assuming a special form of central force interaction between atoms. He began from the Clausius virial law

$$3pV = \overline{\sum r f(r)} + 2\overline{L}$$

where L, r, and f(r) are the kinetic energy, distance between two atoms and the force between two atoms respectively. The product rf(r) is summed over all pairs of atoms and a mechanical time average taken. Mie assumed the force f(r) to consist of a cohesive term of the van der Waals type and a repulsive term increasing more rapidly with distance, to prevent the collapse of the lattice under the attractive forces. He therefore used for a potential

$$\phi(r) = \phi_1(r) + \phi_2(r)$$

$$= -\frac{a}{r^m} + \frac{b}{r^n} \qquad [n > m] \qquad \ldots . \; 2.13$$

where a, b, m, and n are constants. Equation 2.13 is the simplest law expressing the interaction between two atoms: at large values of r the first, attractive term alone is

effective and at small values of r the second, repulsive term dominates. For isotropic regular lattices it can be shown[4] that in equilibrium, if the potential of a gram atom is Φ_o then

$$\Phi_o = \phi_{o1} + \phi_{o2} = -\frac{A}{V^{m/3}} + \frac{B}{V^{n/3}} \qquad \ldots . 2.14$$

where $A = \frac{a}{2} s_m N^{1+\frac{m}{3}}$, $B = \frac{b}{2} s_n N^{1+\frac{n}{3}}$, s_m and s_n are lattice sums; they are functions of the lattice structure and m and n only, and independent of any isotropic distortion.

Expanding Φ_o in terms of the atomic displacements from the equilibrium position, the terms of first order are zero from symmetry conditions and the second order terms, representing the potential energy of vibration, have an average value which is, by the laws of mechanics, equal to the average value of the kinetic energy. So that

$$\bar{\phi}_1 + \bar{\phi}_2 = \phi_{o1} + \phi_{o2} + \bar{L} \qquad \ldots . 2.15$$

The kinetic energy will be shared between the repulsive and attractive forces and so can be written

$$\bar{\phi}_1 = \phi_{o1} + \mu \bar{L}$$

$$(\mu < 1). \qquad \ldots . 2.16$$

$$\bar{\phi}_2 = \phi_{o2} + (1-\mu)\bar{L}$$

The force f(r) will be given by

$$f(r) = -\frac{\partial \phi}{\partial r} .$$

Summing this over all pairs of atoms

$$\overline{\sum rf(r)} = m\overline{\sum \phi_1} + n\overline{\sum \phi_2}$$

$$= m\bar{\phi}_1 + n\bar{\phi}_2$$

$$= m\phi_{01} + n\phi_{02} + [m\mu + n(1-\mu)]\bar{L} \quad \ldots . 2.17$$

Putting this into the virial law equation it becomes

$$3pV = m\phi_{01} + n\phi_{02} + (2 + m\mu + n[1-\mu])\bar{L}$$

and gives the equation of state

$$pV = -V\frac{\partial \bar{\Phi}_0}{\partial V} + \gamma 2\bar{L} \quad \ldots . 2.18$$

where $$\gamma = \frac{1}{3}\left(1 + \frac{m\mu}{2} + \frac{n}{2}[1-\mu]\right) \quad \ldots . 2.19$$

Mie's equation of state is obtained from this by putting m=3, since Mie wrongly supposed that the van der Waals forces were proportional to $1/r^3$, and used the classical value of $L = \frac{3}{2}RT$. Neglecting the contribution of attractive powers, i.e. $\mu=0$, this transforms 2.18 into

$$pV + \frac{A}{V} - \frac{n}{3}\frac{B}{V^{n/3}} = \frac{n+2}{2}RT \quad \ldots . 2.20$$

Gruneisen assumed $2\bar{L} = E = \int_0^T C_v \, dT$

and gave the equation of state as

$$pV + \frac{m}{3}\frac{A}{V^{m/3}} - \frac{n}{3}\frac{B}{V^{n/3}} = \gamma E$$

or writing $G(V) = \frac{m}{3}\frac{A}{V^{m/3}} - \frac{n}{3}\frac{B}{V^{n/3}}$

$$pV = -G(V) + \gamma E \qquad \ldots . 2.21$$

where E is any function of Θ/T and not the special Debye form for the energy. Gruneisen, in a very thorough discussion of this equation, extended the theory to the limit imposed by using the given approximations. Some of the results he obtained will be used later in a discussion of thermal expansion. Gruneisen extended this theory to include metals, despite the use of interatomic potentials known to have no physical significance in metallic solids. Even for the simplest molecular crystals such as the solidified inert gases where the electrons do not in general greatly influence the physical properties, the use of a potential such as Mie's (equation 2.13), is merely an approximation to the theoretically derived interatomic potential.

For a metallic crystal, where the interaction of the electrons with the lattice is many times greater, this approximation is not theoretically justifiable. It does

however, form the basis of a theoretical developement which is extremely useful in a comparison of experimental data, while remaining mathematically simple and easy to manipulate.

2.5 Equations of state based on lattice dynamics.

Born developed the Debye theory, extending it explicitly to molecular and ionic crystals where the crystal lattice contains more than one particle per unit cell. The theory was based on the investigation of the vibration spectrum of a one-dimensional linear chain of diatomic molecules.[24] The solution of the equations of motion is generally in two parts: one associated with the low frequency or acoustic vibrations and the other with high frequency or optical vibrations. For a three-dimensional lattice with s particles per unit cell there are three acoustic branches and (3s-3) optical branches. Born applied Debye's theory to the acoustic branches and for the optical frequencies, substituted the values corresponding to the high frequency ends of the optical frequency bands and used the Einstein formula for the energy (cf. eqn. 2.6). The energy of the crystal per mole is then[25]

$$E = RT\left\{ \sum_{j=1}^{3} \int D(\theta_j/T)\,\frac{d\Omega}{4\pi} + \sum_{j=4}^{3s} P(\theta_j/T) \right\} \quad \ldots\ldots 2.22$$

where if c_j is the wave velocity and $\omega_j = 2\pi\nu_j$

$$D(x) = \frac{3}{x^3}\int_0^x \frac{\xi^3\, d\xi}{e^{\xi}-1}, \qquad \xi = \frac{h\nu}{kT} \qquad \ldots\ldots 2.23a$$

$$P(x) = \frac{x}{e^x - 1}, \qquad x = \frac{h\nu_m}{kT} \qquad \ldots\ldots 2.23b$$

$$\theta_j = \frac{h}{k} c_j \sqrt[3]{3/4\pi\Delta} \qquad j = 1, 2, 3. \qquad \ldots\ldots 2.23c$$

$$\theta_j = \frac{h}{k}\nu_j^{\circ}, \qquad j = 4, 5, 6 \ldots 3s. \qquad \ldots\ldots 2.23d$$

The addition of Einstein terms has meaning only as long as the optical branches are approximately monochromatic and the ν_j can be replaced by ν_j°. For ionic forces this approximation has been shown to be poor by Blackman.[26] Numerical calculation from 2.22 is difficult because of the dependence of c_j on direction. If one substitutes for the average value of $D(\theta_j/T)$ the Debye expression already found, then equation 2.22 is identical with Debye's.

The work of Born and von Karman was extended by Born to a general theory of vibrations of crystals.[27] He calculated the energy of the crystal in a standard state of rest by summing the potential energy per unit cell over the lattice and considering small homogeneous displacements of

the lattice particles. He obtained an expression for the free energy in terms of the external forces, atomic displacements and the temperature.

This theory formed the foundation of Blackman's treatment of the vibration spectra of lattices, in which he calculated the vibration spectra of face-centred (f.c.c.) and body-centred (b.c.c.) cubic lattices.[28] This theory was developed still further by Fine, Kellerman, Montroll and Leighton.[29][30][31][32] Little work has been done directly relating these investigations to the equation of state of a solid.

Born and his co-workers developed a number of equations of state using Boltzman statistics so that the theory is valid only where the free energy is proportional to the product of the eigenfrequencies, that is for $T>\Theta$. The equation of state of a b.c.c. lattice was obtained by Furth[33] and later for the f.c.c. lattice by Bradburn and Gow.[34][35] Bradburn gave a rigorous discussion of a f.c.c. lattice using the special force potential

$$\phi = \frac{u n m}{n-m}\left\{-\frac{1}{m}\left(\frac{r_0}{r^{\ell}}\right)^m + \frac{1}{n}\left(\frac{r_0}{r^{\ell}}\right)^n\right\}, \qquad n>m \quad \ldots \quad 2.24$$

where u is the minimum potential energy for a pair of atoms at the equilibrium separation distance r_0, and obtained the

equation of state using the high temperature approximation for the free energy

$$F = \Phi_0 + kT \sum \ln (h\nu_j / kT).$$

Furth compared this equation of state with expermental values and showed that it gave good agreement.(2)

Bradburn's equation was given as

$$p = \frac{2k\theta}{V_0} (1+\xi)^{3/2} \left\{ 17.24 + \frac{T}{\theta} F(\xi) \right\} \qquad \ldots . 2.25$$

where V_0 is the volume at p=0, T=0,

$$1 + \xi = \left(\frac{V_0}{V} \right)^{\frac{n+m}{3}}, \qquad n = 2m = 12$$

$$F(\xi) = \frac{2}{1+\xi} + 2.44 - 4.01\xi + 6.59\xi^2 - 10.34\xi^3 + 17.09\xi^4 \ldots$$

For a comparison between experimental results, the Gruneisen theory is more direct and the condition $T > \theta$ limits the usefulness of equation 2.25 to high temperatures.

2.6 Electronic and anharmonic effects

In the work already described, anharmonic effects and the effects of the conduction electrons have been neglected. The Debye theory takes account of anharmonicity in as much as it allows a variation of θ with volume and Gruneisen and Mie, in developing their equation of state, assumed a

temperature dependent lattice constant. As yet, however, no complete theory of lattice vibrations has been carried through satisfactorily for a three-dimensional ionic crystal, much less a three-dimensional metal. In the harmonic theory the oscillator frequencies ν_j are independent of the lattice constant, a. However in taking higher than first order potential terms into consideration, then the coefficients of the second order potential terms are functions of a. If in the expansion of ϕ,

$$\phi = \phi_1 + \phi_2 + \phi_3 + \phi_4 + \cdots$$

terms higher than quadratic ones are omitted, then part of the anharmonic effect is already described by the dependence $\nu_j(a)$. This is known as the quasi-harmonic approximation.

A summary of the developement of anharmonic theories has been given by Dobbs and Jones[53] ranging from the anharmonic theory of a linear one-dimensional chain by Damkohler to that of Domb and Zucker for the argon close-packed cubic lattice, where the thermodynamic properties α, C_p, K_T and γ were calculated using a method due to Henkel. An extensive review of the theory of anharmonic effects in crystals by Leibfried and Ludwig[55] considers only ideal crystals. The basis for discussion is the Born-Oppenheimer approximation

in which the nuclei are considered as being in a potential due to the average effect of the electrons. The potential energy of the nuclei can be expanded for small displacements and in the harmonic theory considered earlier, all terms higher than second order are dropped. The anharmonic theory takes into account higher terms also.

Leibfried and Ludwig, after a general discussion of anharmonic theory, go on to determine the thermal expansion from a quasi-harmonic expression for the free energy. The variation of the ν_j with strain is replaced by a spectral average $\overline{\nu_j^2}$ which is calculated from the potential expression as was first done by Born.[57] This is exact for a model with central forces acting between nearest neighbours only but otherwise is not exact, except for the Debye spectrum in low and high temperature limits. For consideration of thermal expansion this approximation may not be tenable. The approximation of an average $\overline{\nu_j^2}$ value is equivalent to substituting the generalised frequency dependent Gruneisen constant $\gamma(\nu)$ by a mean value and using this approximation, it is shown that the thermal expansion is proportional to the internal energy and hence on this basis the expansion coefficient is proportional to the specific heat, as is expected with a constant value for $\gamma(\nu)$. At very low

temperatures this approximation can be quite poor since at low temperatures, only the low frequencies are excited. If the actual $\gamma(\nu)$ differ at low frequencies from those at high frequencies or from the mean value, then this becomes apparent as a deviation of the expansion coefficient from proportionality to the specific heat. This has been calculated by Blackman for special models of the potential and is discussed in section 2.8 below.

The influence of the anharmonicity on the specific heat at low temperatures has scarcely been investigated. One should not expect the harmonic theory to hold even at very low temperatures. Because of the zero point vibration, the influence of anharmonicity does not disappear even at absolute zero. In a description of the temperature variation of the specific heat using the above approximation for the ν_j^2 for the high temperature specific heat, and using the Debye spectrum and potential terms up to fourth order to calculate the specific heat and Debye Θ for the limiting case $T \to 0$, it is shown that the specific heat, as before, is proportional to T^3 but the Debye Θ differs from the value calculated on the harmonic theory even at very low temperatures.[55] This throws some doubt on the validity of Daniels's calculation of the Gruneisen γ_0 described in section 2.8.

2.7 Approximations for γ and Gruneisen's treatment of thermal expansion

To obtain an expression for the thermal expansion of regular monatomic crystals, Gruneisen developed the equation of state at constant pressure. From equation 2.21 if p=0 then

$$G(V) = \gamma E.$$

Expanding G(V) in powers of $V - V_0 = \Delta$

$$G(V) = G(V_0) + \Delta G'(V_0) + \frac{\Delta^2}{2!} G''(V_0) + \ldots$$

It can be shown that(25)

$$G(V_0) = 0$$

$$G'(V_0) = \frac{1}{\chi_0}$$

$$G''(V_0) = -\frac{m+n+3}{6} \frac{1}{V_0 \chi_0}$$

and it follows that

$$G(V) = \frac{\Delta}{\chi_0} \left\{ 1 - \frac{m+n+3}{6} \frac{\Delta}{V_0} + \ldots \right\} = \gamma E \quad \ldots . 2.26$$

By neglecting the second term in 2.26 and using the

resulting expression for Δ as a correction factor, one has

$$\Delta = \frac{\gamma E \chi_o}{1 - \frac{m+n+3}{6} \frac{\gamma E \chi_o}{V_o} + \ldots}$$

and writing $Q_o = V_o/\gamma\chi_o$

$$\frac{\Delta}{V_o} = \frac{E}{Q_o\left\{1 - \frac{m+n+3}{6} \frac{E}{Q_o}\right\}} \qquad \ldots . 2.27$$

Gruneisen showed that $\partial E/\partial T)_p$ had a value lying between C_p and C_v and approximating it by C_v, obtained for the thermal expansion

$$\alpha = \frac{C_v}{Q_o\left\{1 - \frac{m+n+3}{6} \frac{E}{Q_o}\right\}^2} \qquad \ldots . 2.28$$

This equation was used by Nix and McNair in a discussion of the thermal expansion of pure metals.[46] They found that values of θ required to fit the theory to their experimental results, agreed reasonably well with those given by the Debye theory of specific heats as was predicted by Gruneisen. Values of $(m+n+3)/6$ are compared below with those obtained theoretically by Gruneisen, who calculated values with $m=3$, $n=6\gamma-2$ and

$$\gamma = -\frac{V}{C_v} \frac{\partial V/\partial T}{\partial V/\partial p} .$$

	$\frac{m+n+3}{6}$ Gruneisen[4]	$\frac{m+n+3}{6}$ Nix and McNair[46]
Cu	2.7	2.8
Al	2.8	2.7
Ag	2.4	2.4
Au	3.7	3.4
Fe	2.3	3.7
Ni	2.6	4.0

The poorer agreement for Ni and Fe is probably caused by the large electronic contribution to the thermal expansion which was disregarded by Nix and McNair when fitting equation 2.28 to their experimental results.

Equation 2.27 was used by Pullan[11] to discuss his results on thermal expansion since it removes the necessity of approximating $\partial E/\partial T)_p$ by C_v: E was calculated by graphical integration of experimental values of C_v. From his results, Pullan concluded that Gruneisen's law did not hold at low temperatures below about 40°K.

Slater[47] derived γ using the Debye theory and assuming Poisson's ratio independent of volume. This gave

$$\ln \nu_m = \frac{1}{6} \ln V - \frac{1}{2} \ln \chi + \text{constant}.$$

Defining

$$\gamma_D = - \frac{d \ln \nu_m}{d \ln V} ,$$

$$\gamma_s = - \frac{2}{3} - \frac{1}{2} V \left(\frac{\partial^2 p}{\partial V^2} \right)_T \Big/ \left(\frac{\partial p}{\partial V} \right)_T \qquad \ldots . 2.29$$

$$= \frac{1}{2} \frac{d \ln (\chi / V^{1/3})}{d \ln V} ,$$

Slater compared these equations with experimental values and obtained fairly good agreement. He pointed out however, that Poisson's ratio should increase with temperature so that γ would also tend to increase with temperature and γ_0 (the value of γ as T tends to zero), would be less than γ_∞ (the value of γ as T tends to infinity). Barron[48] showed that γ_s from equation 2.29 is not related to the γ derived from experimental values of thermal expansion using the equation

$$\alpha = \frac{\chi_T \gamma C_v}{V} .$$

They are, however, of the same order of magnitude, as shown by Slater.

2.8 Recent theoretical developements.

The general equation of state 2.3 reduces to the Gruneisen form if all the γ_j are equal and Gruneisen's law can be considered as postulating that this is true for all solids. In this case Gruneisen's equation of state 2.21 follows at once. The γ_j are generally not all equal, but this equation forms a useful basis for a discussion of the temperature variation of γ.

Bijl and Pullan[7], in a discussion of the thermal expansion of solids based on the Debye-Brillouin model, showed that it followed from Gruneisen's equation of state that for high temperatures γ (equal to γ_∞) will be constant but that at low temperatures below about $0.3\theta_D$ variation in γ should be expected until at very low temperatures γ again is constant with a value γ_0 depending on the velocities of transverse and longitudinal waves in the solid. They treated a crystal of N particles as an elastic isotropic continuum with N longitudinal and 2N transverse waves possible, all with the same cut off wavelength (but different cut off frequencies for the longitudinal and transverse waves). They found characteristic temperatures θ_l and θ_t for both types of vibrations, giving

$$\gamma_l = -\frac{d \ln \nu_l}{d \ln V}, \qquad \gamma_t = -\frac{d \ln \nu_t}{d \ln V},$$

where ν_ℓ and ν_t are the longitudinal and transverse wave velocities respectively. These were substituted in the equation

$$\frac{\Delta V}{V_o} = A\gamma \frac{E}{1 - bE}$$

neglecting the second term in the denominator. E was given by

$$E = RT\left[D(\theta_\ell/T) + 2D(\theta_t/T)\right]$$

where D(x) is as in equation 2.23 and γ was then given by

$$\gamma = \frac{3\gamma_\infty}{1 + 2\gamma_t/\gamma_\ell} \frac{D(\theta_\ell/T) + 2(\gamma_t/\gamma_\ell) D(\theta_t/T)}{D(\theta_\ell/T) + 2D(\theta_t/T)} .$$

This gave γ constant at high and low temperatures with $\gamma_o > \gamma_\infty$.

In a further paper, Bijl and Pullan included the effect of the conduction electrons on the thermal expansion of metals by adding a term to the free energy.[36] Using the relation

$$\frac{\alpha}{\chi} = -\frac{\partial^2 F}{\partial V \partial T}$$

they showed that

$$\frac{\alpha}{\chi} = \frac{\gamma_\ell C_\ell + \gamma_e C_e}{V} \qquad \ldots . 2.30$$

where C_ℓ and C_ϵ are the lattice and electronic specific heats, and if T_ϵ is the characteristic temperature of the conduction electrons then

$$\gamma_\epsilon = - \frac{d \ln T_\epsilon}{d \ln V}$$

$$\gamma_\ell = \frac{\alpha V}{\chi C_\ell} \quad .$$

Defining an effective γ_m for a metal by

$$\frac{\alpha}{\chi} = \frac{\gamma_m}{V} (C_\ell + C_\epsilon) \qquad \ldots . 2.31$$

and comparing with equation 2.30 one obtains

$$\gamma_m = \frac{\gamma_\ell C_\ell + \gamma_\epsilon C_\epsilon}{C_\ell + C_\epsilon} \quad . \qquad \ldots . 2.32$$

At ordinary temperatures $\gamma_m = \gamma_\ell$ since $C_\epsilon \ll C_\ell$, but at very low temperatures where $C_\epsilon > C_\ell$, $\gamma_m \approx \gamma_\epsilon$.

Defining a Gruneisen parameter characteristic of the lattice only by

$$\frac{\alpha}{\chi} = \frac{\gamma_m'}{V} C_\ell \qquad \ldots . 2.33$$

and comparing with 2.30 gives

$$\gamma_m' = \gamma_\ell + \gamma_\epsilon \frac{C_\epsilon}{C_\ell} \qquad \ldots . 2.34$$

At low temperatures

$$\frac{C_e}{C_l} = \frac{5kT}{24\pi^2 \epsilon_o'} \left(\frac{\theta_D}{T}\right)^3 \qquad \ldots . 2.35$$

where[37] $\epsilon_o' = kT_e$.

Thus by plotting γ_m' against $1/T^2$ and extrapolating to $1/T^2 = 0$, γ_l can be obtained as the intercept at $1/T^2 = 0$. γ_e can be obtained from the slope of the line.

Barron considered a more detailed model, defining weighted averages of the γ_j as[6]

$$\gamma(s) = \frac{\sum \gamma_j \nu_j^s}{\sum \nu_j^s}$$

$$= -\frac{1}{s} \frac{d \ln \overline{\nu_j^s}}{d \ln V}$$

where $\overline{\nu_j^s}$ is the s^{th} moment of the frequency spectrum. He showed that $\gamma_o = \gamma(-3)$ and $\gamma_\infty = \gamma(0)$ and obtained expressions for the $\gamma(s)$, estimating $\gamma(0)$ by interpolation. Barron calculated these for a f.c.c. lattice with central forces acting between nearest neighbours only, and showed that γ

varied substantially only for $T \sim 0.2\theta$, the variation being independent of the force law. Considering more distant neighbour interactions he showed that

$$\gamma_\infty - \gamma_0 \leqslant 0.3.$$

Blackman derived an expression for ionic rocksalt-type crystals giving γ in terms of the elastic constants[39] and with

$$\gamma_j = - \frac{d \ln \nu_j}{d \ln V}$$

finds γ_∞ as an arithmetical average of the γ_j and finds γ_0 to be

$$\gamma_0 = \frac{1}{3} + \frac{A c_1^2 + B c_3^2}{2 c_1^2 + c_3^2}$$

where A and B are functions of the elastic constants and c_1, c_3 the velocities of the transverse and longitudinal waves. He estimated that γ should drop by 20% between the high temperature limit γ_∞ and the low temperature limit γ_0. A further investigation[40] of a diamond-type and an ionic lattice, in which the γ_j were obtained from the elastic constants, gave a negative value of γ_0 while $\gamma_\infty = (n+2)/6$ was positive. The negative values of γ_0 for the diamond-type lattice were not dependent on the choice of parameters

and were negative in all cases. Negative values of γ_0 were also found for an alkali halide model lattice when the shear modulus was small. These calculations, however, refer to the lattice models considered. For practical applications it appears that the occurrence of negative γ is limited to the diamond-type lattice. Some evidence for this is given by the results of Novikovo[41][42] who found for germanium, negative values of the expansion coefficient below $\sim 48^{\circ}K$ and that the expansion of diamond became negative at $\sim 90^{\circ}K$. Gibbons[43] found the expansion of silicon negative below $120^{\circ}K$ but for germanium did not report a drop of the expansion coefficient below zero, although at the lowest temperature measured ($\sim 40^{\circ}K$) it was very small. He has also found negative values of the expansion coefficient for vitreous silica.[54]

In a consideration of two-dimensional ionic lattices[44] Blackman showed that although negative values of γ_j occurred they were small for the two-dimensional case, with values depending on the exponent n of the repulsive part of the potential. The average over the lattice γ_0, however, was never negative even for very large n. It appears nevertheless that variations in γ are to be expected with variations of 30% possible. White[19] has measured the thermal expansion

coefficient of KCl down to 4°K and calculates $\gamma_\infty = 1.47$ and $\gamma_\infty - \gamma_0 = 1.13$, a variation of ~ 75%. The most rapid variation of γ is at $\sim 0.13\theta_D$ agreeing with Blackman's estimate. On a preliminary measurement of the thermal expansion of NaCl, White obtained $\gamma_0 = 0.94$ and $\gamma_\infty - \gamma_0 = 0.61$, a change of ~ 40%.

Horton introduced anharmonicity into Born's lattice dynamics by allowing the elastic constants to vary with volume.(45) He found γ_∞ by Barron's method of averaging the γ_j. To find the variation with temperature, Leighton's central force theory(32) was used together with experimentally determined values of the elastic constants. The model suggests $\gamma_0 < \gamma_\infty$ with $\gamma_\infty - \gamma_0 \approx 0.5$. The contribution of the conduction electrons was not considered except in the variation of the elastic constants. The theory gives good agreement with White's results for copper at low temperatures but at high temperatures γ is larger than experimental values would suggest.(18)

Daniels has calculated the low temperature limit of γ for germanium and silicon on the assumption that the Debye theory holds at very low temperatures.(49) He calculated the value of θ_0, (the value of θ_D as T tends to zero), from

the elastic constants, molar volume and density, using de Launey's tables[50] and calculated γ_0 from

$$\gamma_0 = - \frac{d \ln \theta_0}{d \ln V}$$

obtaining for

Ge - $\gamma_0 = 0.49$

Si - $\gamma_0 = 0.25$.

Gibbons has measured the thermal expansion of germanium and silicon down to 40°K and has calculated γ.[48] The results he obtained are reproduced in Fig.1, showing his extrapolated values for γ which make γ_0 zero at T=0. This seemed the obvious thing to do since γ for both germanium and silicon was negative. It appears, however, from Daniels's calculation that γ may become positive again at very low temperatures. No experimental confirmation of this has yet been produced and it is not at all certain that Daniels's extrapolation is theoretically justified.[55]

Barron and Klein have shown that the free energy of an anharmonic crystal at low temperatures is given by an effective harmonic distribution and that the values of θ_0 calculated from harmonic theory and anharmonic theory are

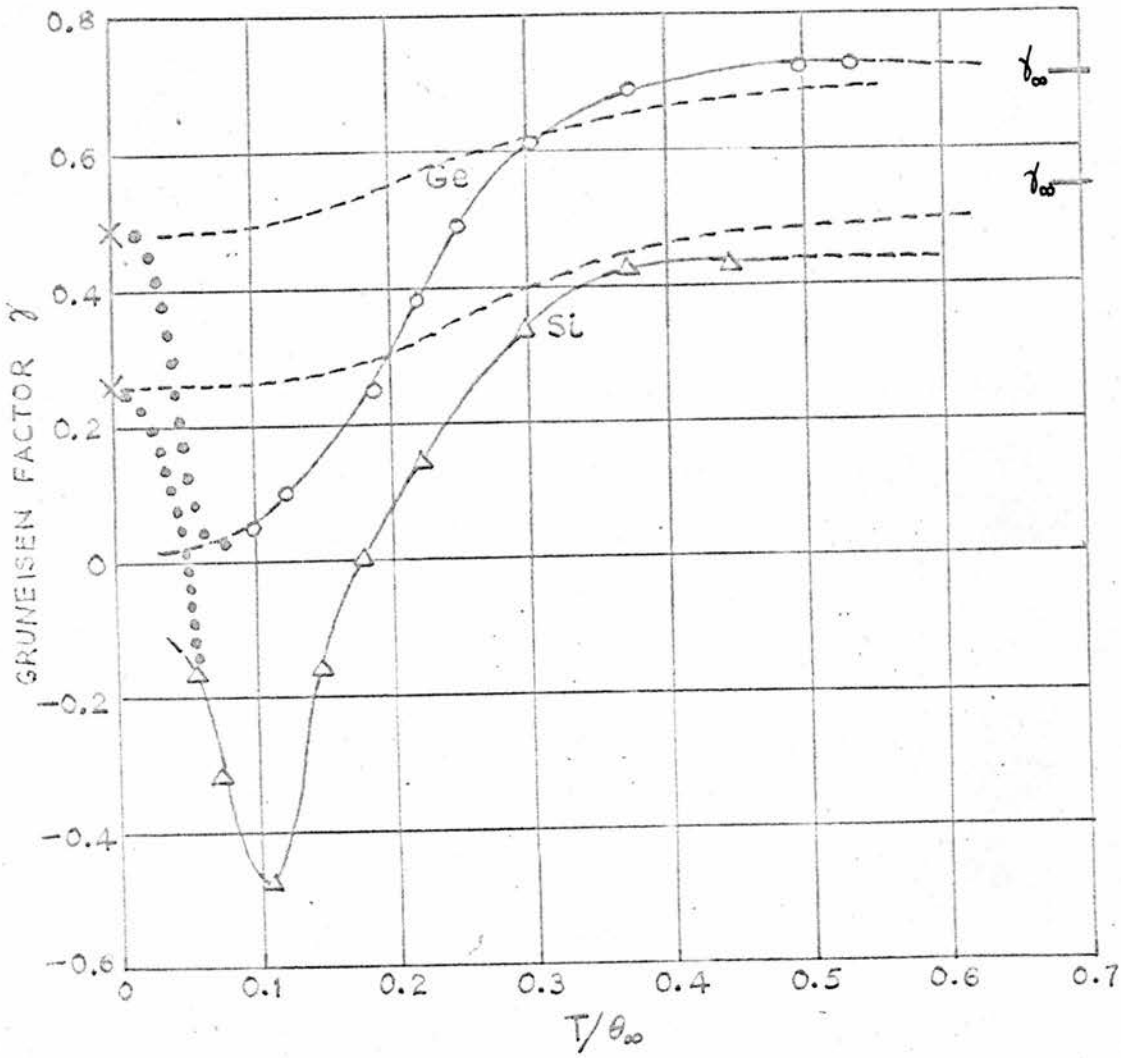

γ as a function of T/θ_∞ for Ge and Si: —○—, —△— Gibbons (refs. 43, 54); ---- Collins (ref. 56); .... Daniels's extrapolation to calculated values of γ_0 (ref. 49).

Figure 1 - Thermal expansion of Si and Ge.

equal.[58] They suggest that the discrepancy between the two theories is due to the approximations made in the treatment, especially the use of the average value for the ν_j^2 as described in section 2.6.

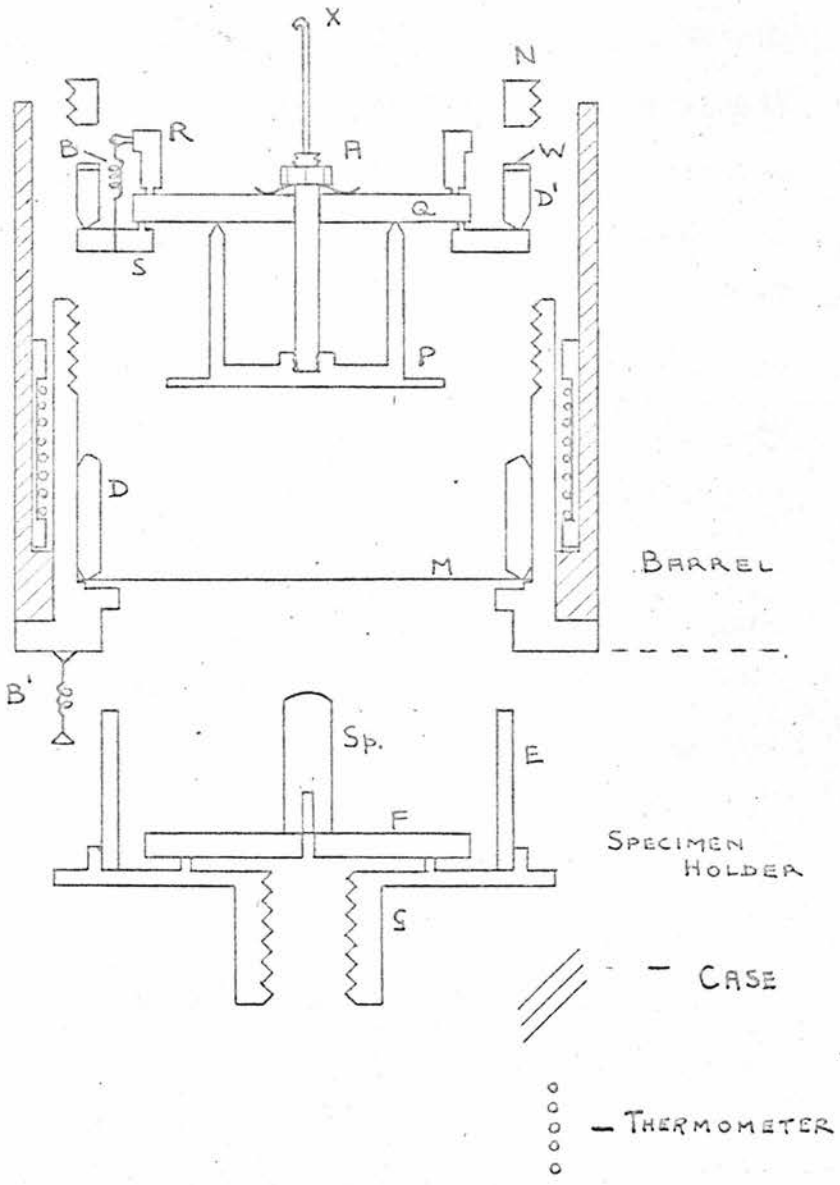

Figure 7 - The dilatometer.

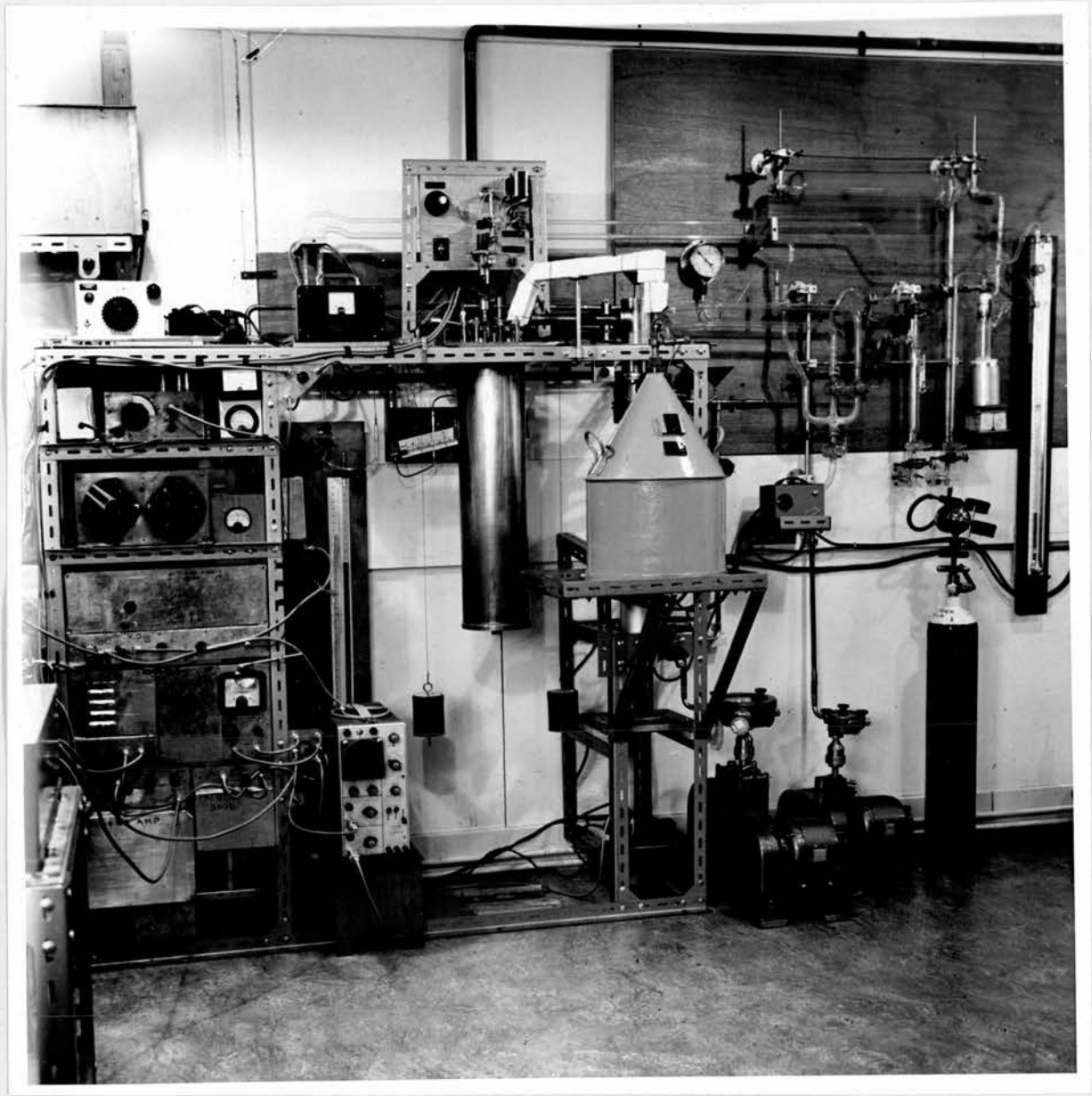

Figure 2 - General view of the apparatus.

CHAPTER 3

THE APPARATUS

This chapter will give details of the experimental apparatus: a detailed account of the construction of the cryostat and associated electronics is given elsewhere by Stewart.[12] The author worked with Stewart for some time during the test runs described by him (ref.12, p.70ff.). This time was spent getting to know the apparatus and its low-temperature performance, and assisting generally in the experimental work. In his thesis (ref.12, p.79), Stewart attributes the large scatter in the experimental data to buckling of the phosphor bronze membrane described below in section 3.4. It was at this point that the apparatus was taken over by the present author.

It seemed much more likely that the cause of the apparent instabilities was the low Q-value of the resonant circuit. It was possible to 'sit' on the resonance peak anywhere within a hundred or so cycles per second and obtain zero deflection on the phase sensitive detector. The first modification was to replace the ferrite-cored

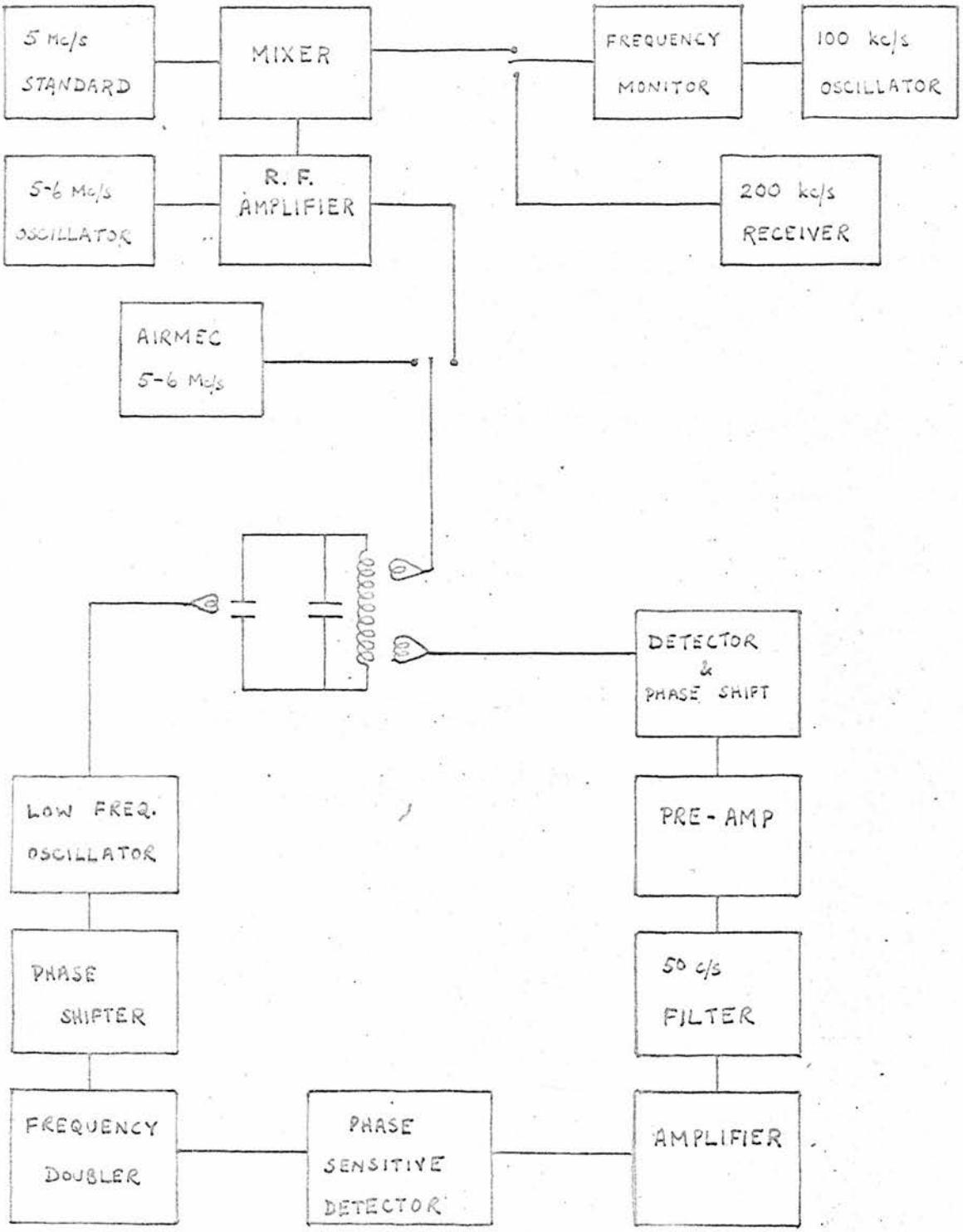

Figure 3 - Block diagram of the apparatus.

inductance described in Chapter 1.3, by a coil and vibrating reed condenser described below (section 3.3). Apart from the addition of a volume control the low frequency amplifier was left unchanged as was the frequency doubler, mixer, phase sensitive detector and frequency measuring equipment. The variable oscillator (section 3.9) was modified by replacing the tuned load buffer stage removed by Stewart and shunting the anode load coil to give a level frequency response. The detection system was redesigned as described in section 3.7. An automatic filling mechanism was added (section 3.12) and the vacuum system modified by the addition of magnetic safety valves.

3.1 Basic principles of measurement.

The basic principle of the apparatus is described by Bijl and Pullan.[36] The specimen whose expansion is to be measured determines the separation between the plates of a condenser in a resonant circuit. The resonant frequency of the circuit is thus fixed by the length of the specimen and by suitable calibration can be related to the change in distance between the plates, which equals the required length change of the specimen. To obtain the desired accuracy of measurement the resonant circuit must have as high

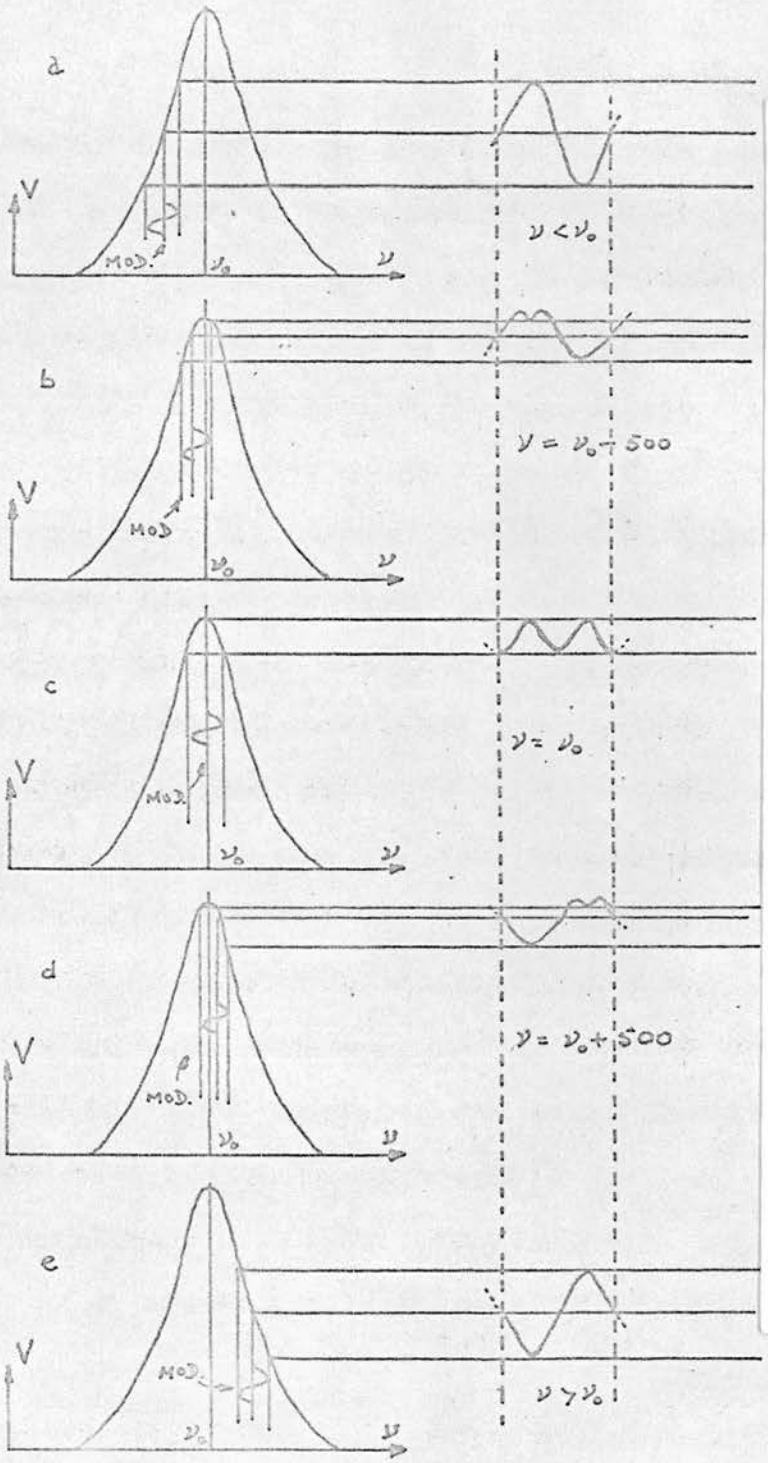

Figure 4 - The principle of detection.

a Q-value as possible.[11]

The resonant circuit consists of a coil in series with a capacity formed by the dilatometer capacity and a vibrating reed condenser in parallel. The vibrating reed condenser causes the frequency at which the circuit resonates to oscillate about a fixed value: this is equivalent to keeping the circuit resonant frequency constant and varying the input frequency but removes the need for a frequency-modulated oscillator. What happens can be seen most easily by considering Fig.4. At frequencies less than ν_0 the radio-frequency voltage across the inductance is amplitude modulated at the frequency of the vibrating reed condenser; likewise at frequencies greater than ν_0 the radio-frequency is modulated but the modulation is 180° out of phase with that below ν_0. Thus the modulation changes phase as the frequency is swept through resonance. At resonance the modulation frequency is doubled since the frequency is swept through resonance twice in each cycle. The resonance frequency is found by comparing the modulation with the vibrating reed exciting signal, using phase-sensitive detection.

3.2 The cryostat.

The cryostat consists essentially of three containers surrounded by a large can (1, Fig.5), which is pumped to

provide a thermal vacuum at a pressure of 0.05mm.Hg. The three cans contain liquid nitrogen (2,Fig.5), liquid hydrogen or helium (3,Fig.5), and the dilatometer. The dilatometer can (4,Fig.5) is self-contained and vacuum tight so that it can be pumped independently of the outer can and filled with a thermal exchange gas to ensure thermal equilibrium of the specimen and dilatometer. The coil and vibrating reed condenser of the resonant circuit are mounted on top of the liquid nitrogen can so that they are kept at a constant temperature. The three inner cans can be linked by two mechanical heat switches to bring the temperature of the dilatometer to the required point.

3.3 The resonant circuit.

The coil consists of 20 turns of 18 s.w.g. enamelled high conductivity copper wire wound on a glass former, diameter 3cm. and 8cm. long. The former was covered with a layer of shellac before the coil was wound and two more layers of shellac added after winding the coil. The coupling coil for the radio-frequency input and the signal pickup coil were both wound at the same end of the former since placing them at opposite ends of the main coil reduced the Q of the resonant circuit by a factor of ten. This is probably due to the coupling between the input and pickup

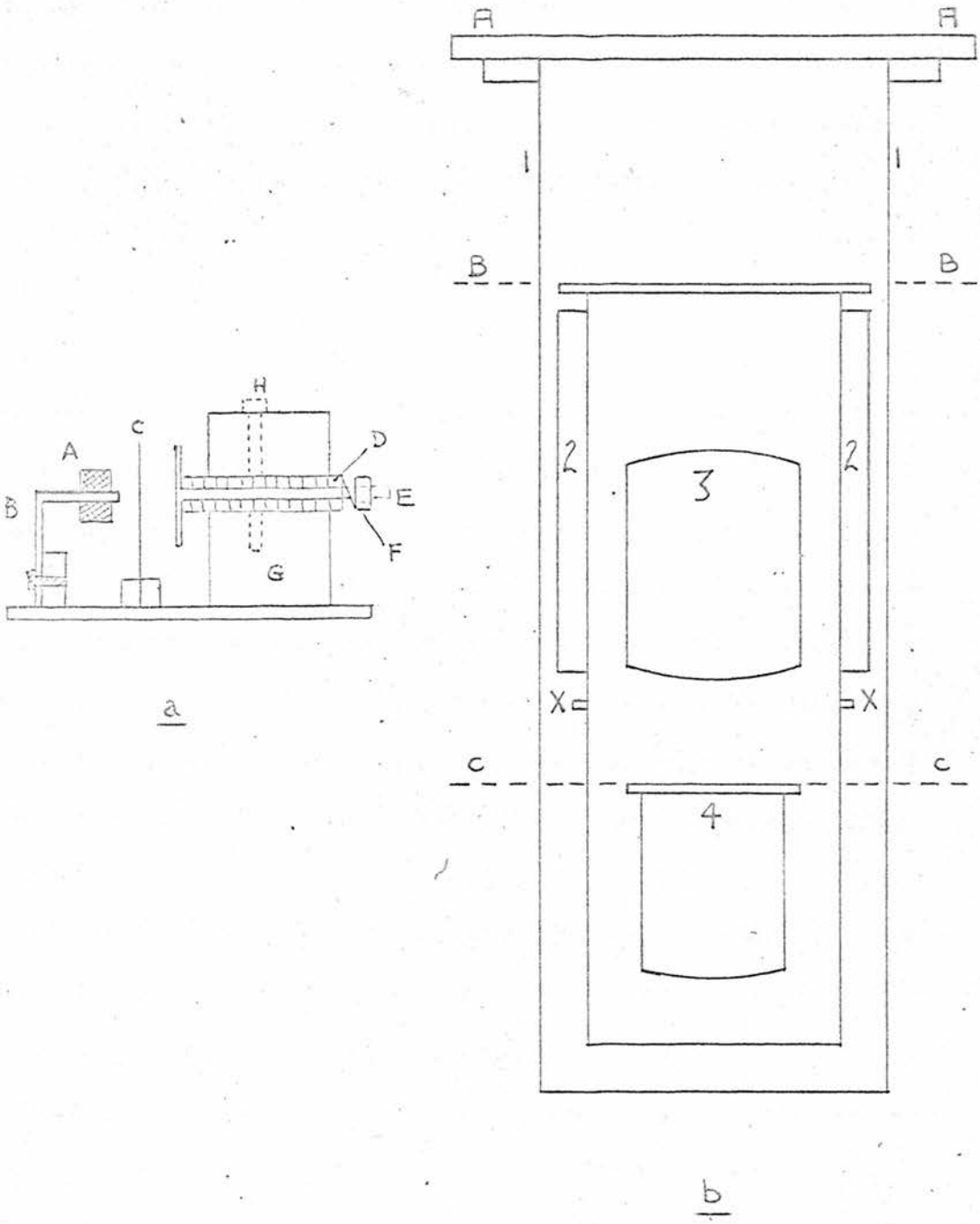

Figure 5 - The vibrating reed condenser and cryostat.

coils, both of which have an earthed end. Both these coils consisted of two or three turns of 40 s.w.g. enamelled copper wire. The Q of the main coil was 200 dropping to 100 in the resonant circuit inside the cryostat, because of the earth capacity effect of the metal outer can and metal supports for the electrical connections to the coils. On cooling the coil to liquid nitrogen temperatures the Q of the circuit rose to 150. The coaxial line down the centre of the cryostat, which was originally eureka, was replaced by 30 s.w.g. enamelled copper wire to reduce the ohmic resistance of the circuit.

The vibrating reed condenser was constructed on a brass plate which was bolted to the top plate B-B of the liquid nitrogen can (Fig.5). The reed C was a length of 0.005in. thick spring steel 0.5in. wide, clamped at one end to the brass plate. The fixed plate was a copper disc soldered to a length of screwed brass rod E and insulated from its support by a sheath of tufnol D. The whole plate assembly was held together by a spring washer and nut F on the screwed rod. The insulating sleeve was firmly clamped in a split brass block G which was soldered to the brass base plate. The top section of the block was held down by spring loaded screws H to allow for contraction of the insulating

sleeve on cooling to liquid nitrogen temperatures. The length of the reed was adjusted until its resonant frequency was about 320c/s and it was driven by a small electromagnet A, wound with 48 s.w.g. double cotton covered copper wire. The sensitivity is reduced by having the vibrating reed condenser in parallel with the dilatometer capacity, by a factor

$$\frac{c}{c + c_v}$$

where c includes the dilatometer capacity and stray earth capacities and c_v is the average value of the vibrating reed condenser. Hence it is desirable to keep c_v as small as possible. c_v was approximately 1pF with c about 70pF, thus reducing sensitivity by less than 2%.

3.4 The dilatometer.

The dilatometer was machined from a single block of high conductivity copper. The main body of the dilatometer consists of three concentric cylinders (Fig.7): the outer case and inner case, and between them the platinum resistance thermometer. At the lower end of the inner case, a 0.002in. thick circular phosphor bronze membrane M rests on a projecting ledge and is clamped by a copper ring D. A copper ring S rests on the clamping ring D and supports a quartz

plate Q, held between S and a second copper ring R by three phosphor bronze springs B. The whole inner assembly is firmly held by another clamping ring D', a washer and a screwed brass ring N. The top plate P of the dilatometer condenser hangs from the quartz plate and is held against it by a spring loaded nut A. When the dilatometer is assembled, the gap between the membrane and the top plate is $\sim$ 0.35mm. The specimen stands on a copper plate F supported on the base plate G. A copper spacing ring E separates the base plate from the main body of the dilatometer and the specimen holder is supported by three springs B' attached to the main barrel. The length of the spacing ring is adjusted so that the condenser gap at room temperature is about 0.05mm. at the centre of the membrane: this keeps the membrane slightly stretched and reduces the possibility of flexure of the membrane through imperfect annealing and also ensures that the membrane is always in contact with the specimen. The membrane was annealed by heating for three hours at 800°K in a nitrogen filled furnace and allowing the furnace to cool overnight. All parts of the dilatometer are interconnected so that no pressure difference can exist across the membrane.

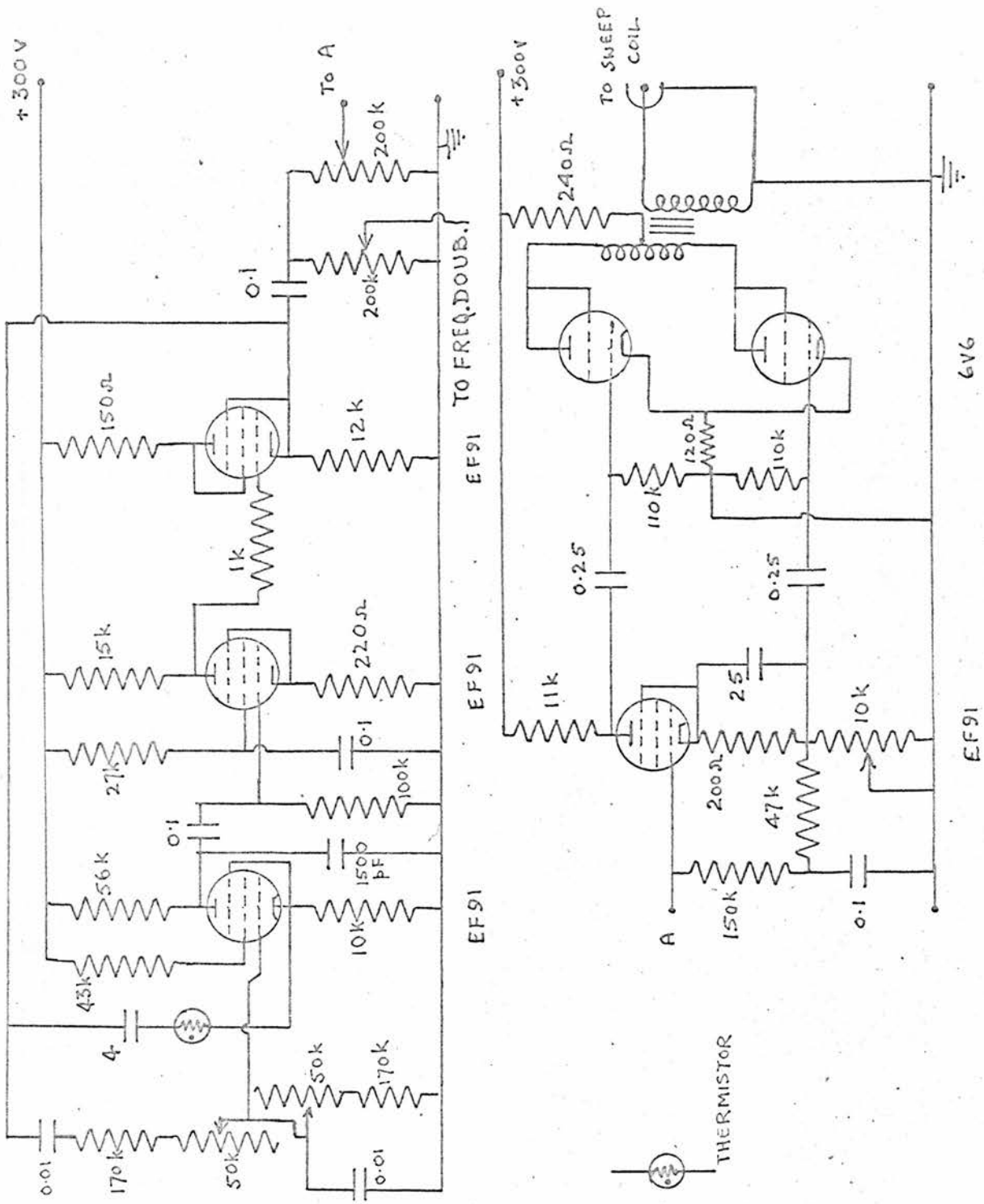

Figure 8 - The low-frequency oscillator.

3.5 The low frequency modulation and reference oscillator.

The vibrating reed condenser was driven by a variable frequency oscillator working in the range 100 - 200c/s (Fig.8). It was a three-stage Wien bridge oscillator feeding via a control potentiometer to a class A push-pull output stage which was transformer coupled to the electromagnet coil. An output was taken between the oscillator and output stages to a phase shifting valve before the frequency doubling circuit.

3.6 The frequency doubler.

The frequency doubler (Fig.9), was required because the vibrating reed was attracted to the electromagnet twice in each cycle and thus vibrated at twice the frequency of the exciting signal. It consisted of a tuned load amplifier tuned to the second harmonic of the low frequency oscillator followed by two stages of narrow band amplification, giving an output of 70 volts r.m.s. maximum.

3.7 Demodulation and signal amplification.

The modulated radio-frequency signal from the pickup coil carried an off resonance modulation of about 5%. The input to the vibrating reed condenser from the frequency doubler required to produce this percentage modulation was

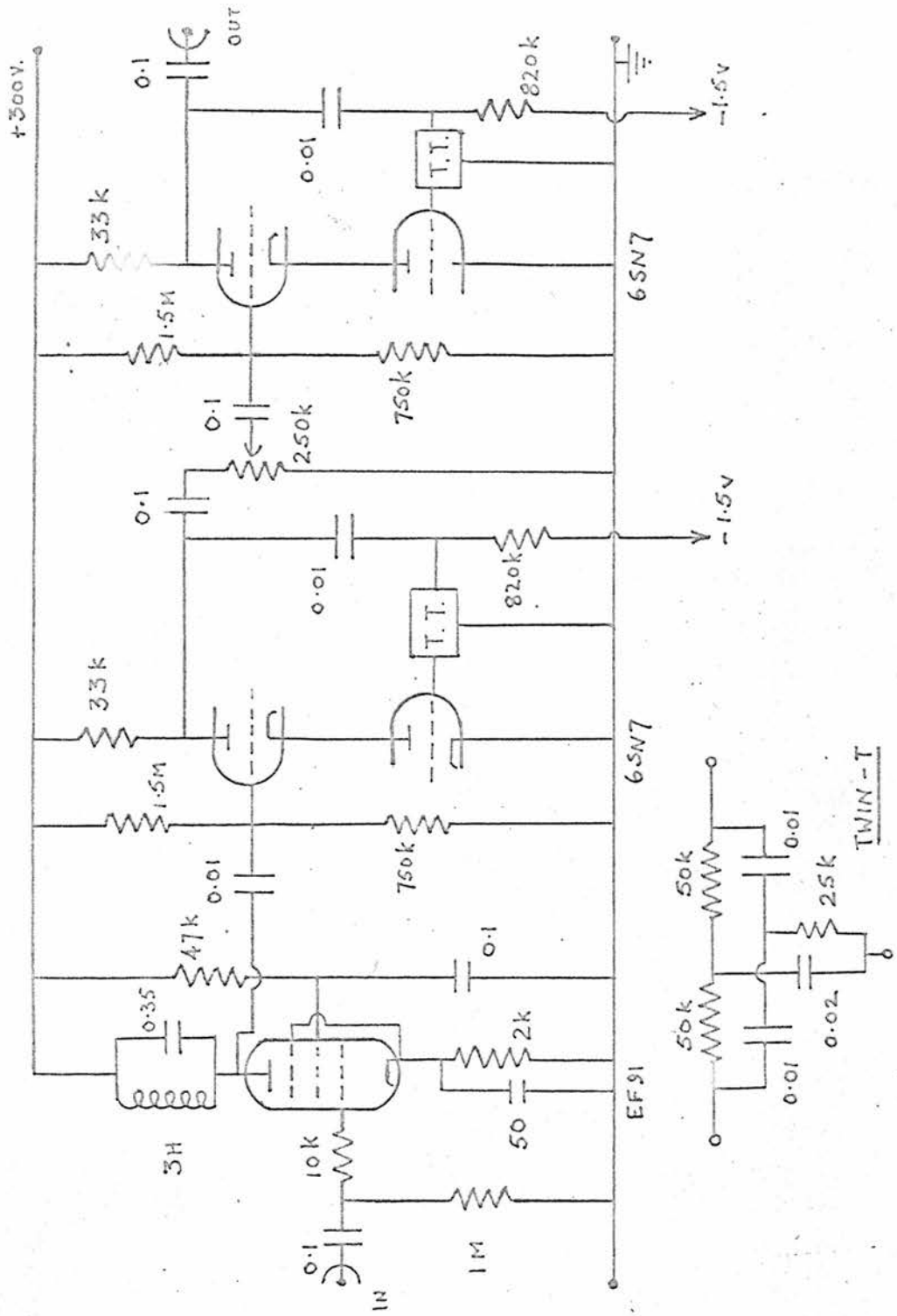

Figure 9 - The frequency doubler.

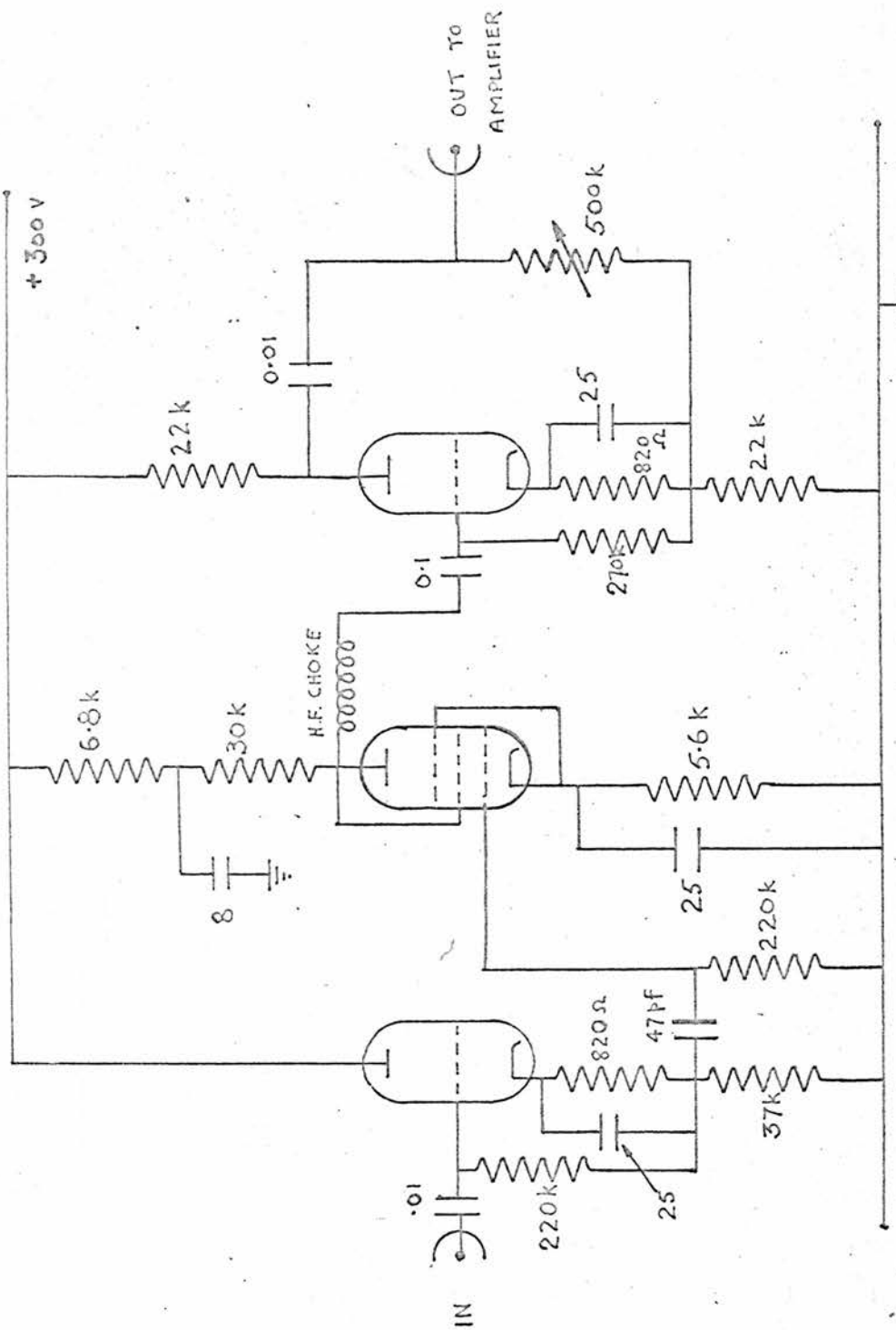

Figure 10 - The detector.

60 volts peak to peak. The modulated radio-frequency signal was fed via a cathode follower to the detector stage which was an EF91 pentode biased to cut off (Fig.10). A radio-frequency choke removed any remaining radio-frequency and the demodulated pickup signal was amplified by a Solartron laboratory amplifier with a gain of 10^4. The amplified demodulated signal had an off resonance magnitude of 8 volts peak to peak. It was found necessary to put a phase shifting stage before the amplifier to enable the phases of the signal and reference voltages to be matched during setting up. The phase of the vibrating reed condenser changes by 180° as the low frequency oscillator passes through the resonant frequency of the reed and since the reed is used off resonance, two stages of phase shift were found desirable. The phase of the signal was adjusted in the initial setting up and thereafter kept constant during an experimental run, any relative phase adjustments being made with the phase shifting stage in the reference voltage generator. The original tuned amplifier following the detector was replaced because it introduced a phase shift in the pickup signal which was dependent on the signal amplitude. Several tuned and narrow band amplifiers were tried including a selecto-jet amplifier(51), but a normal

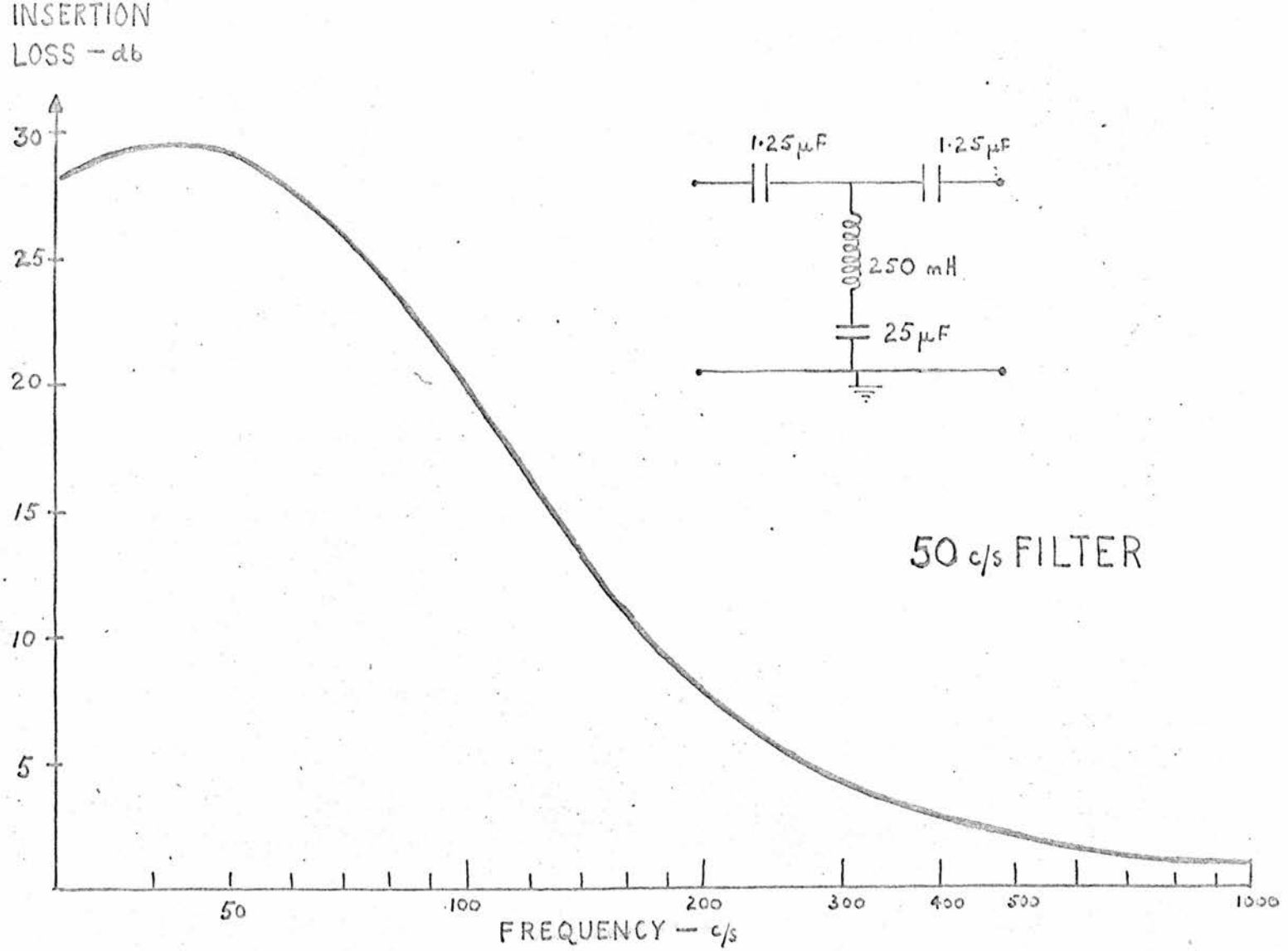

Figure 11 - The 50c/s filter (high-pass).

wide-band amplifier proved most satisfactory. A high-pass filter (Fig.11) was incorporated in the Solartron amplifier to remove the 50c/s pickup on the signal. The pickup was very small but of the same order of magnitude as the modulation on the radio-frequency voltage. Various methods were used to reduce this pickup and some reduction was achieved by using direct current valve heater supplies for the detection and phase shifting stages. Distortion of 0.2 volts at 100c/s was present in the output of the Solartron amplifier with the input short circuited. This arose in the output stages but was within the makers specifications and since it did not interfere with the phase sensitive detector no attempt was made to eliminate it.

3.8 The phase sensitive detector.[52]

Phase sensitive detection was used since it promised to give the best sensitivity.[12] The detector (Fig.12) was a Schuster type described by Stewart. This is basically two valves in parallel in the anode circuit of a third. The two valves are alternately switched on and off by the reference voltage determining which of two resistors R_1 or R_2 carries the anode current of the third valve V_3. Condensers C_1 and C_2 prevent the anodes of V_2 returning to +300 volts when the valves are cut off. A d.c. voltage

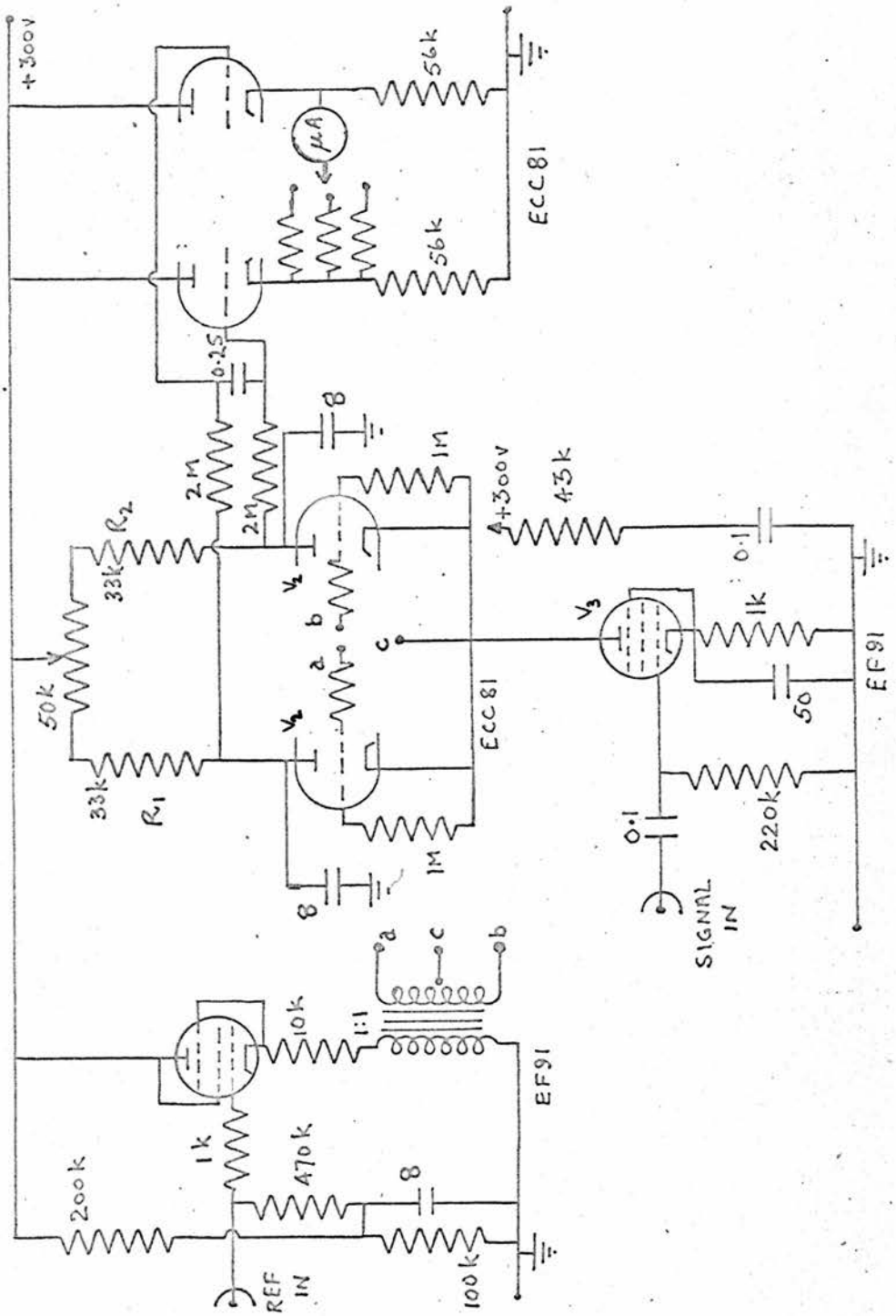

Figure 12 - The phase-sensitive detector.

depending on the phase difference between the reference and signal voltages was taken from the anodes of V_2 via a long time constant circuit and a pair of cathode followers to a d.c. microammeter.

3.9 The variable oscillator and amplifier.

The variable frequency 5 - 6Mc/s oscillator is a push-pull developement of the Clapp type with an L-C frequency determining circuit followed by a tuned amplifying stage providing automatic gain control (Fig.13). The automatic gain control buffer amplifier was originally a straightforward resistive load amplifying stage but it did not provide sufficient gain for automatic gain control purposes and caused instability. The 5.6kΩ resistor shunting the tuned circuit lowers the Q and provides an output which is level within 0.5db. in the 5 - 6Mc/s range. With the original design without the tuned load stage the oscillator output was rather low, ~1 volt r.m.s. and a wide band amplifier was built with a maximum gain of 20 (Fig.14). Two output stages were built to remove the necessity of switching the output from the input coil to the mixer when measuring the frequency. The output to the coil, with the tuned load buffer amplifier and following wide band amplifier, was adjusted to be 5 - 7 volts r.m.s.

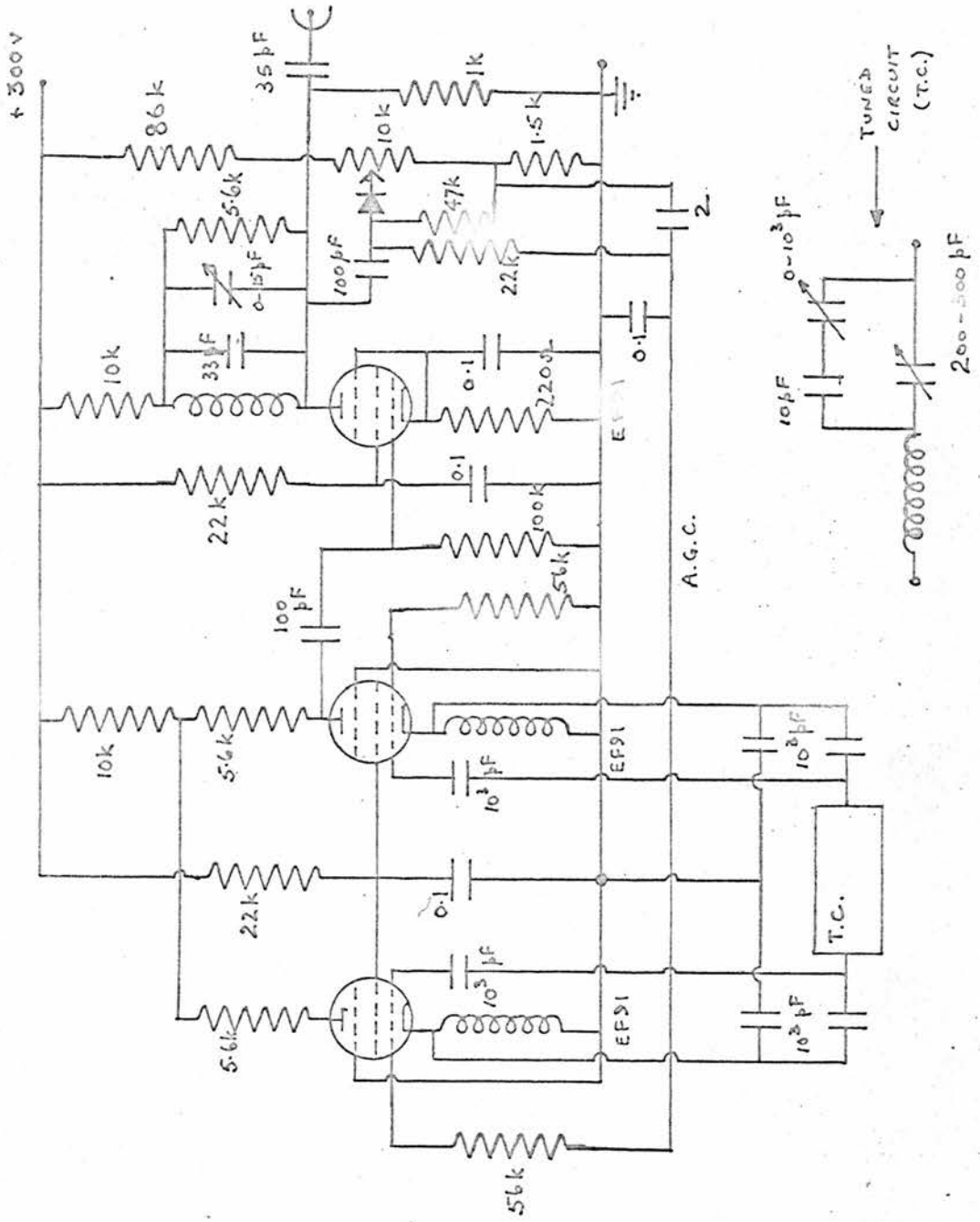

Figure 13 - The 5-6Mc/s variable oscillator.

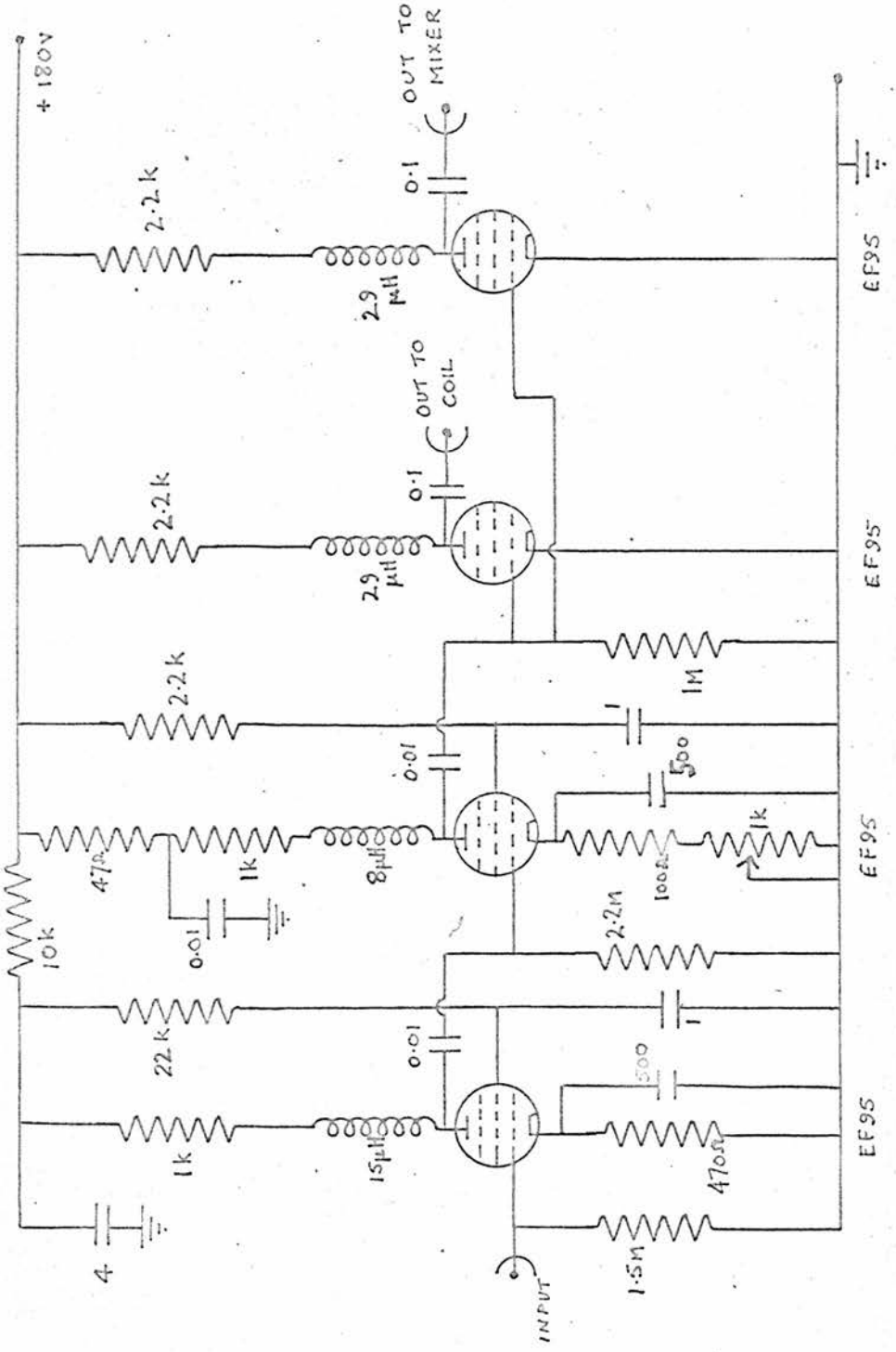

Figure 14 - The 5-6Mc/s amplifier.

3.10 The mixer and frequency measuring equipment.

To measure the frequency of the variable 5 - 6Mc/s oscillator, its output was compared with that of a standard oscillator with a fixed frequency of nominally 5Mc/s, made by S.T.C. and specified to be stable to 4 parts in 10^9. Both outputs were fed to a 6L7G pentagrid mixing valve, the fixed oscillator having two stages of amplification before mixing (Fig.15). A low-pass filter and amplifier provide the beat frequency voltage. The beat frequency was counted on a Cintel frequency monitor which had a maximum counting rate of 1Mc/s. Gate timing pulses were derived from an external 100kc/s quartz crystal controlled oscillator with a long term stability of 1 part in 10^6. The frequency monitor had an interval test circuit for the timing oscillator and the timing intervals were checked by feeding in the B.B.C. 200kc/s standard frequency transmission provided by a receiver (Fig.16).

3.11 Temperature measurement and control.

The dilatometer temperature could be varied between 20°K and room temperature. The temperature was lowered by closing the heat switches, and depending on what liquid is in the lower can the temperature may be reduced to any

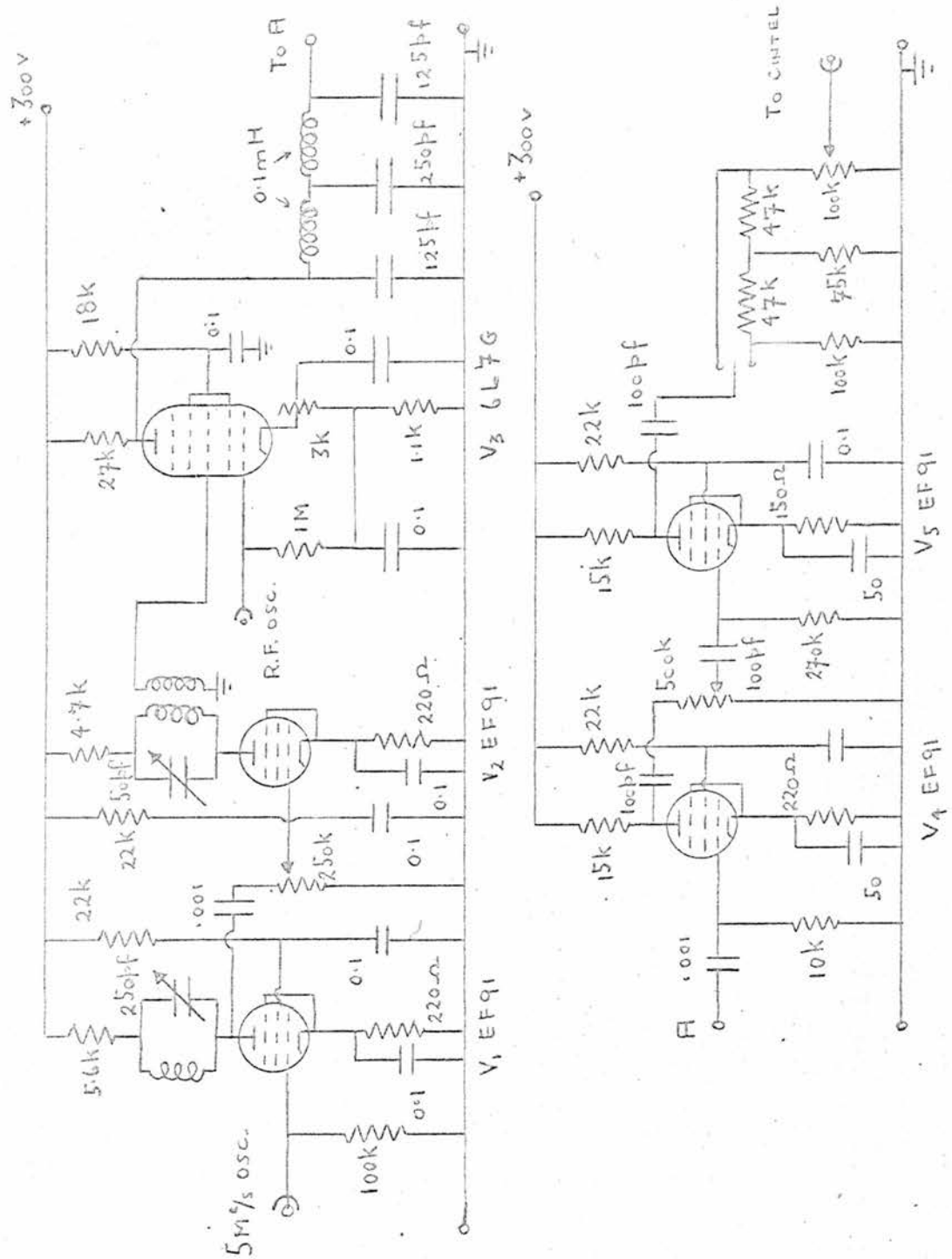

Figure 15 - The mixer.

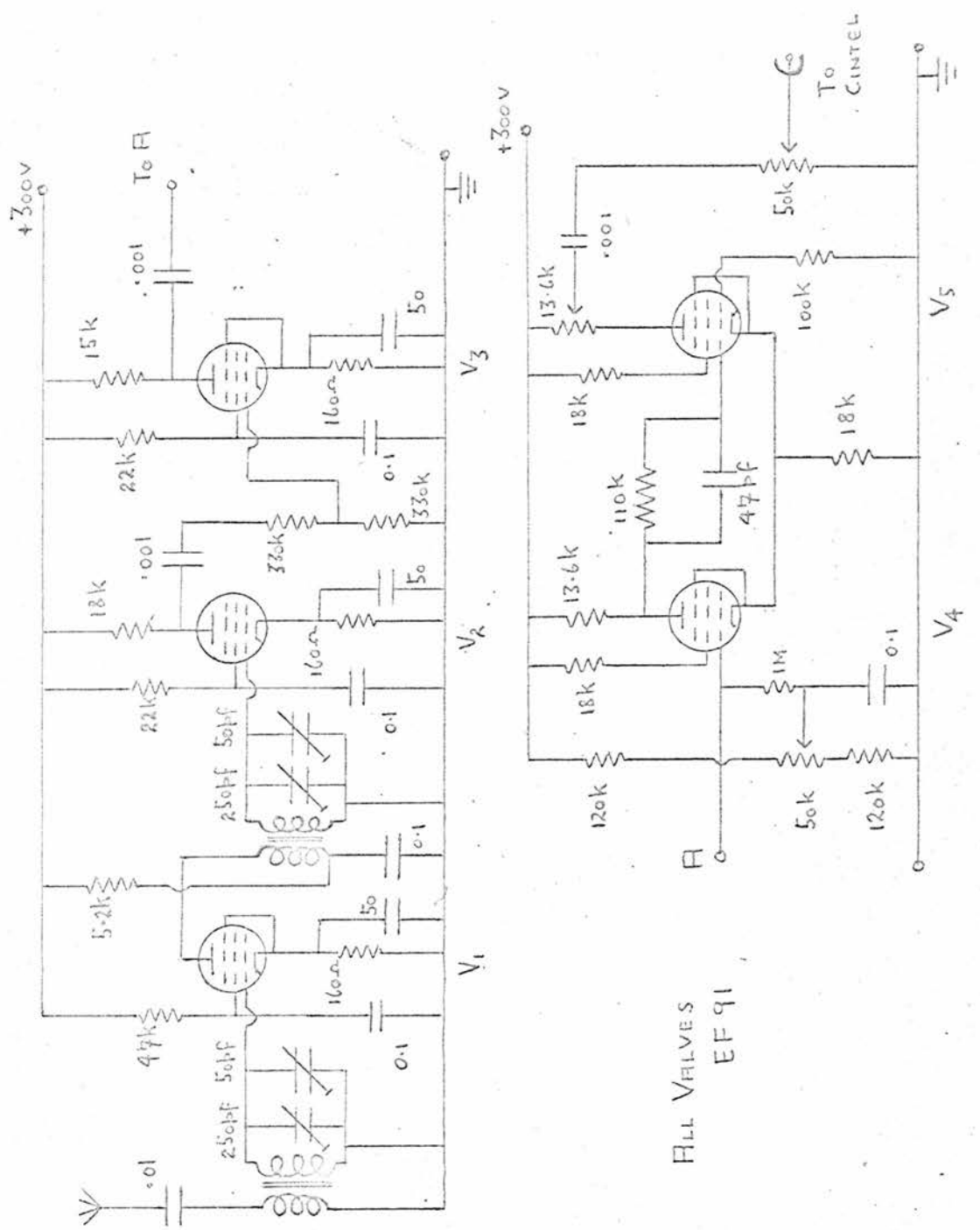

Figure 16 - The 200kc/s receiver.

point between its boiling point and room temperature. When the desired temperature was reached, the heat switches were opened and the temperature held steady by balancing heat losses with a heater wound on the outside of the dilatometer can. The heater supply voltage was derived from a variable transformer giving 0 - 30 volts r.m.s. output, which was connected to the electrical mains supply through a constant voltage transformer to improve the temperature stability. The temperature has been kept constant within 0.01 ^{o}K at a temperature of 220^{o}K for twelve hours without altering the transformer setting.

Thermal equilibrium of the dilatometer and specimen was ensured by filling the dilatometer can with helium at a pressure of a few mm. of mercury and the temperature was measured using the platinum resistance thermometer in the dilatometer. Current through the thermometer was provided by a 2 volt accumulator and was set at 200μA by adjusting the voltage across a 100Ω standard resistance, while a twin galvanometer amplifier was used to measure the voltage across the resistance thermometer enabling temperature changes to be measured to 0.005^{o}K (Fig.17). The resistance thermometer was calibrated using a vapour pressure thermometer mounted on top of the dilatometer can, as described

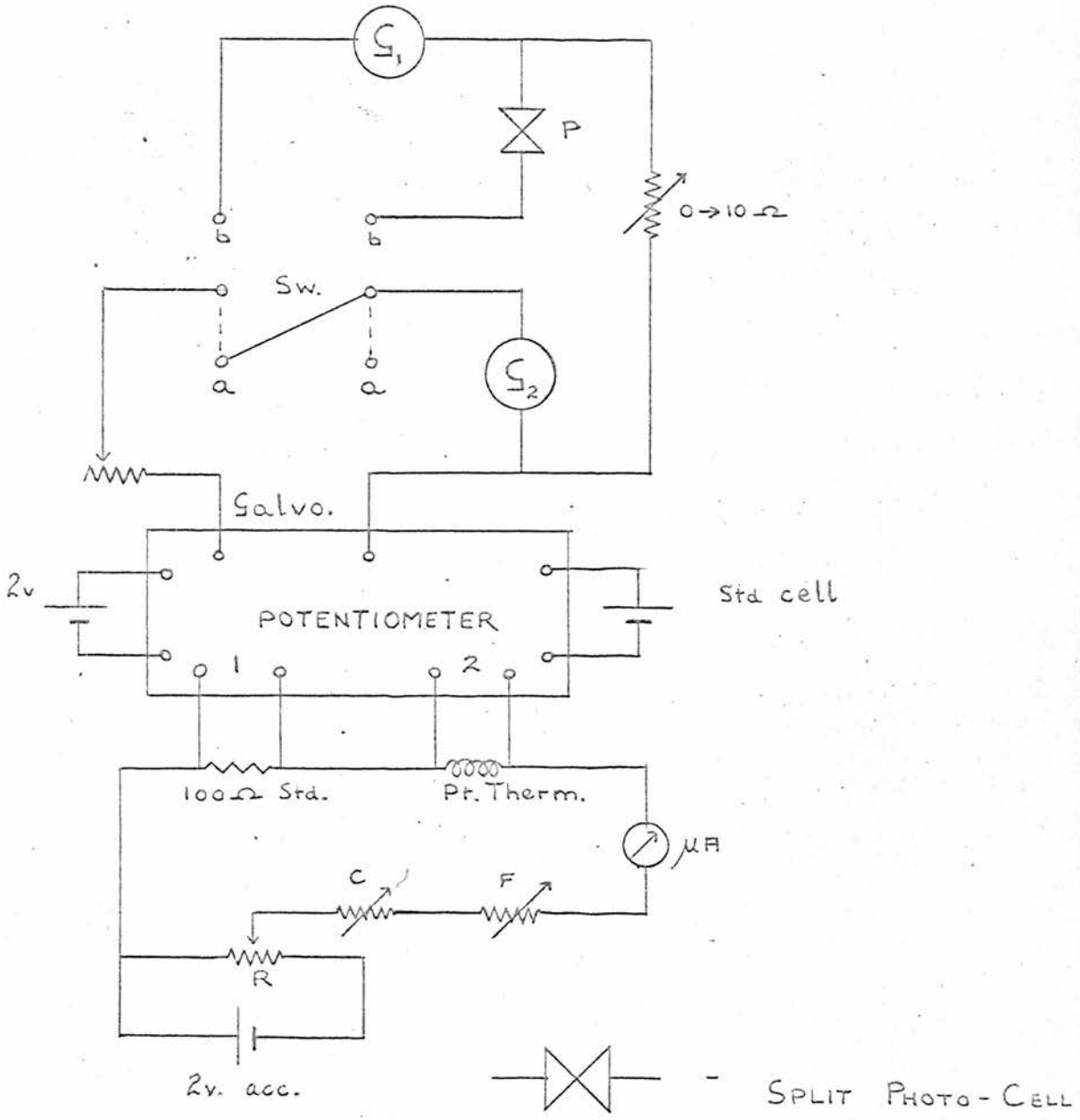

Figure 17 - The temperature measuring circuit.

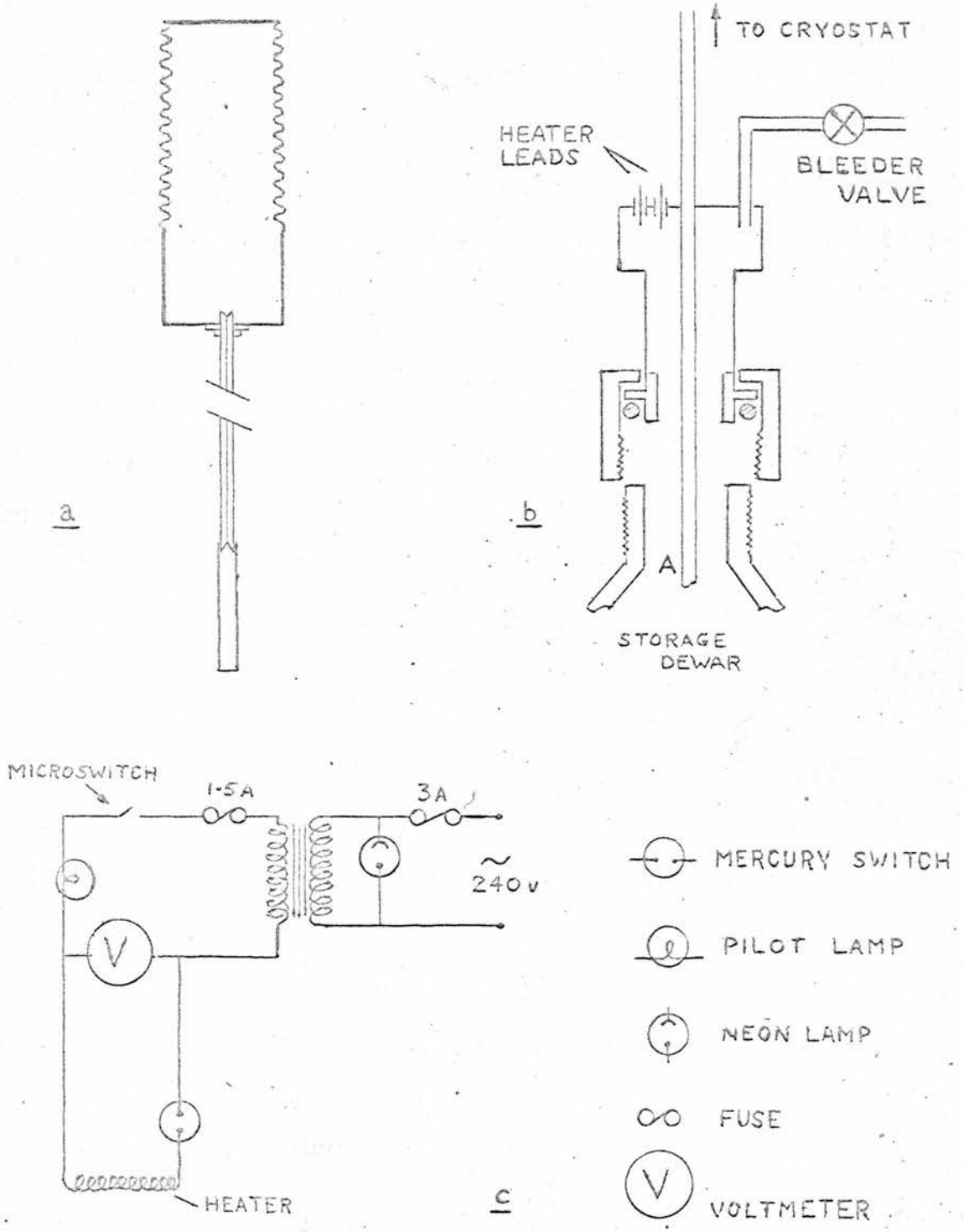

Figure 18 - The automatic filler.

in section 3.13.

3.12 The automatic filling mechanism.

Because of the length of time necessary to complete an experimental run - three or four days - it was decided to incorporate an automatic filler for the nitrogen can so that the apparatus could be left unattended overnight. The sensing element was constructed from a 2in. length of brass bellows tubing 1in. in diameter connected by a length of 3mm. o.d. thick walled copper capillary to a thin walled Cu/Ni bulb (Fig.18a). This was filled with oxygen at a pressure slightly above atmospheric. Oxygen was used as a filling gas so that the filler could be used with liquid oxygen as well as liquid nitrogen. As long as the bulb was immersed in liquid nitrogen the gas inside condenses into the Cu/Ni bulb and the bellows contract. When the liquid level falls below the bulb, heat conducted down the capillary tubing boils off the condensed gas in the bulb and the bellows expand again operating a microswitch. The microswitch completes the circuit of a heater in the nitrogen storage dewar (Fig.18c) and the subsequent pressure rise blows over liquid nitrogen until the bulb is once again immersed. The dewar storage flask was fitted with a bleeder valve

to prevent the pressure rising when the heater was off (Fig.18b). A safety switch was placed in series with the heater to safeguard against a temporary electrical supply failure, with consequent loss of liquid nitrogen from the cryostat because of the thermal vacuum softening and subsequent emptying of the storage dewar. The switch was a small evacuated glass container with two tungsten leads sealed into the top and half filled with mercury. While filling the storage dewar the filling tube A (Fig.18b), to which the switch was attached, was inverted and the switch cooled with liquid nitrogen until the mercury solidified. The filling tube was then inserted in the storage dewar. If the liquid nitrogen should be lost for any reason the temperature will rise only until the mercury liquifies and drops to the bottom of the glass phial, breaking the circuit. The heater consisted of 1 metre of 0.005in. x 1/32in. nichrome ribbon wound on a 3/8in. tufnol former. The heater was run from a 24 volt transformer and gave 36 watts.

3.13 The vacuum system.

The vacuum system can be divided into four sections; the pump for the outside can, the dilatometer pumping system, the vapour pressure thermometer and the hydrogen pumping system.

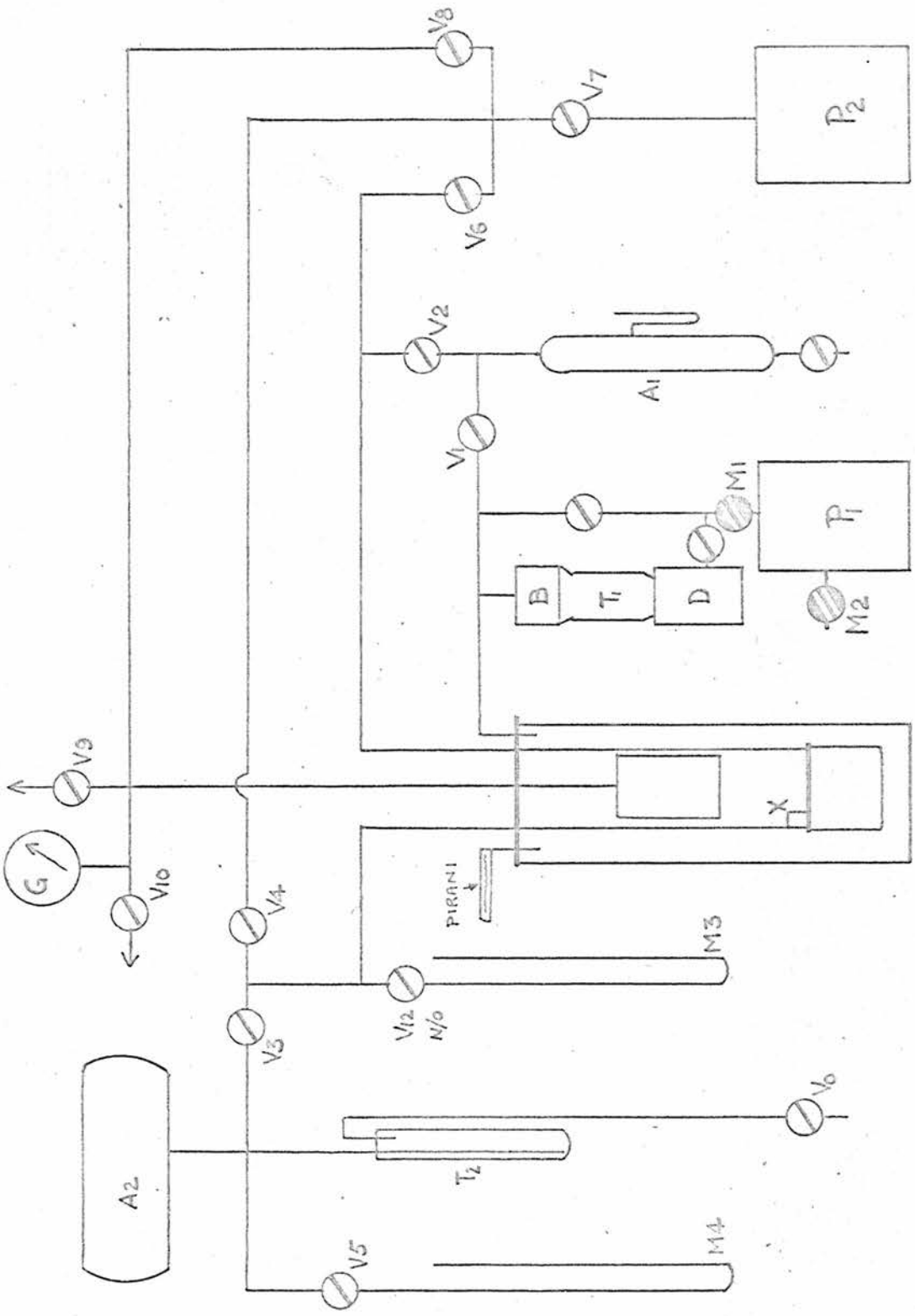

Figure 19 - The vacuum system.

The pumping system for the large outer can serves to provide a thermal vacuum of 0.03 - 0.05mm.Hg. An Edwards silicon oil diffusion pump D is used, backed by an Edwards 1/SC/50/B rotary pump P_1 (Fig.19). This pumping system was also used to pump the dilatometer can and reservoir A through valves V_1 and V_2 after the cryostat was opened to change the specimen. An Edwards mercury vapour trap T was included between the baffle valve B and the diffusion pump D. This was used in place of the original liquid air trap since the Edwards cold trap holds enough liquid air to last for 16 hours without refilling and may thus be used safely overnight. Two magnetic valves, M_1 and M_2 were also added to the original system, one between the diffusion pump and the backing pump and one on the backing pump, to guard the system against electrical supply failure during the periods it was left unattended. These were controlled by a Genevac vacuum protection unit, which in the event of a mains breakdown closes M_1 and opens M_2 after a delay of one second. When the current is restored, M_2 closes first and M_1 is opened after a delay variable between 1/2 and 3 minutes to ensure that the section below M_1 is pumped down to backing pressure.

The dilatometer, after initial pumping, is isolated

by closing V_1 and is filled with helium and pumped down to a pressure of a few mm. of mercury, using pump P_2, an Edwards 2/SC/20/A rotary pump. Once the dilatometer is filled with exchange gas, V_2 can be closed and the helium remaining in the reservoir A_1 used as a heat switch by opening the reservoir to the outer can through V_1, with valve B closed. This method was used occasionally during the initial precooling before each run.

Pump P_2 is also used for pumping the vapour pressure thermometer. This consists of a large reservoir A_2, manometers M_3 and M_4 and the metal bulb X on top of the dilatometer can. This bulb is connected to the main glass system by Cu/Ni capillary tubing. To calibrate the resistance thermometer, the vapour pressure thermometer is filled through V_o and a cold trap T_2, with V_3 and V_4 closed, to a pressure slightly above atmospheric as measured on M_4 with V_5 open. V_3 is then opened for a period of about half an hour to allow the thermometer gas to condense into the bulb X. On closing V_3, the pressure drops until equal to the saturated vapour pressure of the thermometer gas and the pressure is read on manometer M_3.

The liquid hydrogen can is pumped through V_7 and V_8 with V_3 and V_6 closed (using the pump P_2), when using

nitrogen, or by the main laboratory pumping system through V_9 when using helium. V_{10} vents to the open air for use with liquid hydrogen if the pressure in the liquid hydrogen can becomes too high, as indicated by the gauge G.

CHAPTER 4

EXPERIMENTAL PROCEDURE

This chapter will describe the measurements and will give details of the operation of the apparatus.

4.1 Preliminary experiments.

Preliminary experiments, made with this apparatus before the vibrating reed condenser was used to obtain the modulation, have been described by Stewart.[12] During these experiments the modulation of the radio-frequency signal was obtained by a varying inductance in the resonant circuit. A ferrite-cored inductance was used in series with the dilatometer capacity and although this method did not reduce the sensitivity of the circuit resonant frequency to a change in the plate separation, it was found difficult to obtain a very high Q-value and hence the detection of resonance to the required degree of accuracy was not possible. An improvement of a factor of ten in detection sensitivity was achieved by replacing the inductance with a varying capacity as described in section 3.3.

4.2 Measurement of df/dx by micrometer.

df/dx was first measured at room temperature using a dummy glass specimen. A depth micrometer was clamped to the top plate of the dilatometer can, supporting the dummy specimen against the diaphragm. The resonant frequency was measured as the dilatometer gap was increased from zero and values of df/dx calculated from the readings. These are shown in Fig.20, together with the values of df/dx calculated using the diamond specimen (see section 5.1). Agreement is good except at very small gap separations where the micrometer measurements have a large percentage error.

4.3 Calibration of the resistance thermometer.

4.3a The ice point.

The ice point calibration was done by surrounding the dilatometer with ice. The outer can, radiation shield and inner can were removed and a large bucket supported around the dilatometer. This was filled with crushed ice made from distilled water, and readings were taken at intervals for a few hours until the temperature was stable and the resistance had been constant within 0.05% for two hours. The ice point was measured to be 88.025 ohms.

4.3b The oxygen point.

The oxygen point was found using the procedure described

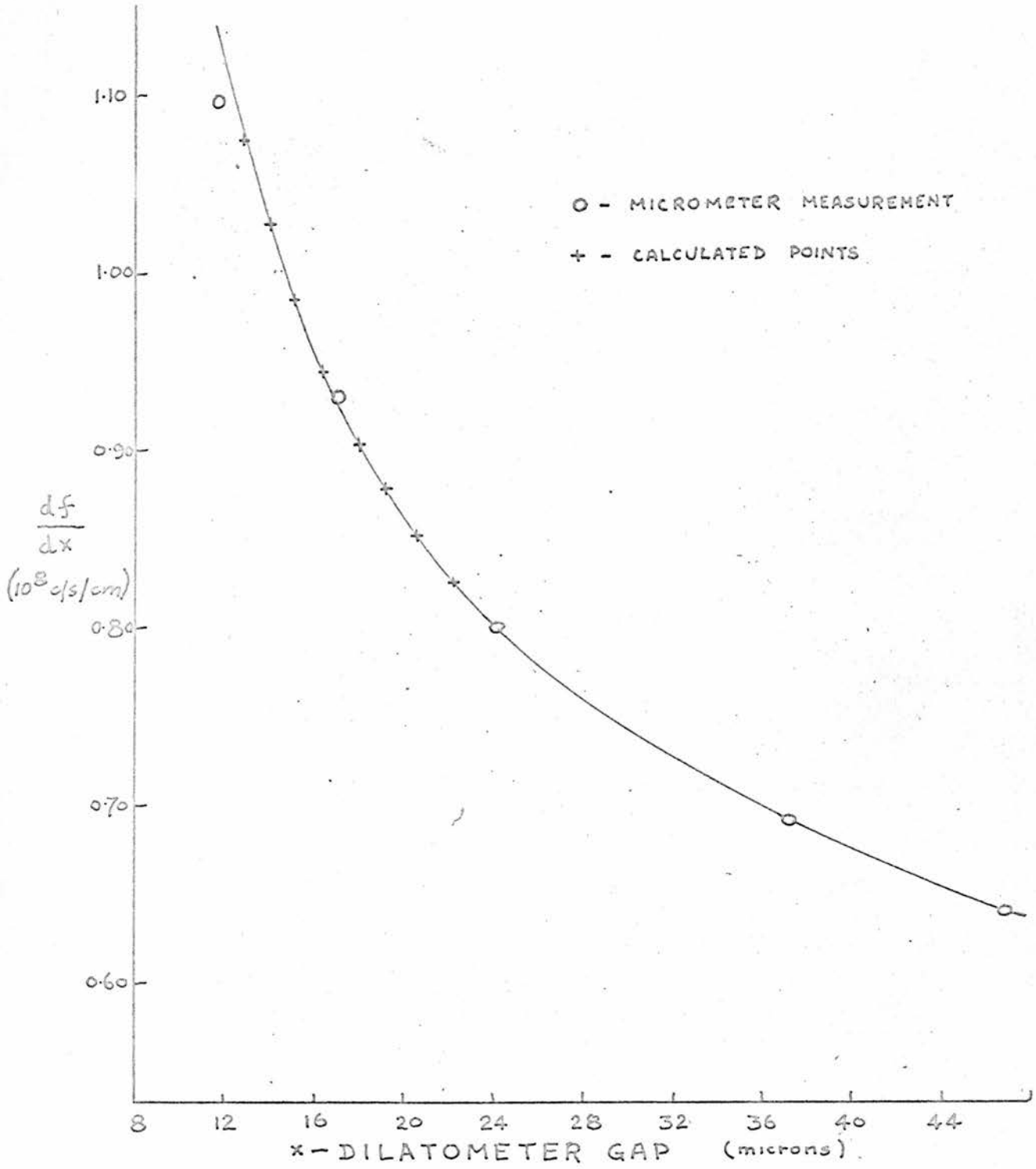

Figure 20 - Graph of df/dx vs. x.

in section 3.13. The vapour pressure thermometer was filled with oxygen through the valve V_o and cold trap T_2. The cold trap was surrounded with a liquid air bath so that oxygen condensed into it together with any higher boiling point impurities. The oxygen was then allowed to boil off slowly, controlling the pressure by adjusting the level of the liquid air bath. When some oxygen had condensed into the thermometer bulb, the thermometer was isolated and the temperature held steady, using the heater if necessary, until the pressure stabilised. The pressure was measured on the manometer and the temperature obtained from saturated vapour pressure tables.

4.4 Measurement procedure and technique.

The preliminary step, while placing the specimen in the dilatometer, was to adjust the resonant frequency of the tuned circuit to be about 5.75Mc/s, by shortening the specimen or the spacing ring D (Fig.7). This was done with very fine grade emery paper and metal polish. When the frequency was set at the required value, the inner can for the dilatometer was replaced. An indium ring seal made from 1/16in. diameter indium wire was used to seal the dilatometer can. This was placed in a groove in the flange of the can while the can was loosely bolted to the top plate

of the dilatometer (C-C,Fig.5), and the can pumped out before finally tightening the bolts as evenly as possible round the circumference. The pressure difference across the seal helped to keep the plate C-C strain free, by holding the can firmly against the plate while the bolts were screwed home.

The heat shield flange was greased with silicon high vacuum grease to ensure good heat contact and bolted to the liquid nitrogen can at X-X (Fig.5). Lastly the outer can was replaced, secured loosely and pumped out before finally tightening the retaining nuts. The whole cryostat was then pumped until a high vacuum was obtained.

The dilatometer was isolated and filled with helium exchange gas to a pressure of approximately 1.5cm. of mercury and the vacuum in the outer can watched to make sure that the dilatometer indium seal was vacuum tight. The upper can was then filled with liquid nitrogen, the heat switches closed and the dilatometer was cooled down to 100°K at a cooling rate of between 12°K and 15°K per hour. Once the dilatometer temperature reached 100°K the heat switches were opened and the dilatometer heater switched on. The heating rate was increased from an initial rate of approximately 5°K per hour to a final rate of 30°K

per hour, the entire warming up taking about eight hours. This precooling was done after experience showed that consistent readings were not obtained unless this was carried out. The dilatometer was stabilised at 270°K and the first frequency and temperature readings noted.

To take a frequency measurement once the temperature was stable, the phase sensitive detector was set on the coarse range and the variable 5 - 6Mc/s oscillator adjusted until a large deflection was obtained on the 100-0-100 d.c. microammeter. The frequency must then be at some point on the Q-curve as in Fig.4a, and the phase shifters were adjusted to make the deflection a maximum. When the deflection is a maximum, the two signals must have a phase difference of 180°. The variable oscillator was then adjusted to bring the deflection to zero, using first the coarse frequency control and then the fine frequency control until the deflection was shown as zero on the most sensitive range of the phase sensitive detector. The phase change should then be 90° for the signal with respect to the reference voltage and the frequency should be set at resonance as in Fig.4c. Both signal and reference voltages were monitored continuously on a double beam oscilloscope, to make the frequency adjustments easier, and photographs

taken at the equivalent points are shown in Fig.4 beside the diagrams. The upper trace is the signal input to the phase sensitive detector (~8 volts), and the lower trace is the modulation voltage input to the coil (~60 volts).

Frequency readings were not made until the temperature had stabilised, when the frequency readings were taken every minute until the readings were consistent and within 10c/s of each other, and no drift was seen on the phase sensitive detector microammeter. The heat switches were then closed and the temperature reduced by 15°K and allowed to stabilise once more. The average cooling rate was 10°K per hour and three quarters of an hour was required for the frequency and temperature to stabilise. Readings were taken at 15°K intervals until the temperature reached approximately 100°K. The dilatometer was then warmed to room temperature once more and readings repeated at 30°K intervals to check the first set of readings.

Several difficulties became obvious during preliminary runs. The inductance and self capacity of the resonant circuit coil was very temperature dependent causing the resonant frequency, at a given dilatometer gap, to depend on the coil temperature. The coil was mounted on the top of the upper can and hence liquid nitrogen

was used in the upper can rather than liquid air which had been used during much of the initial testing. The coil temperature was thus maintained at the boiling point of liquid nitrogen. During the initial runs, it was also found that it was not possible to drive the vibrating reed condenser at its natural vibration frequency, since it was impossible to set the driving oscillator frequency exactly on the reed resonant frequency and a short term vibration of up to 50 per cent of the modulation amplitude occurred. The reed was thus driven just off resonance, where the reed vibration frequency was stable and the amplitude of vibration provided a reasonable signal amplitude.

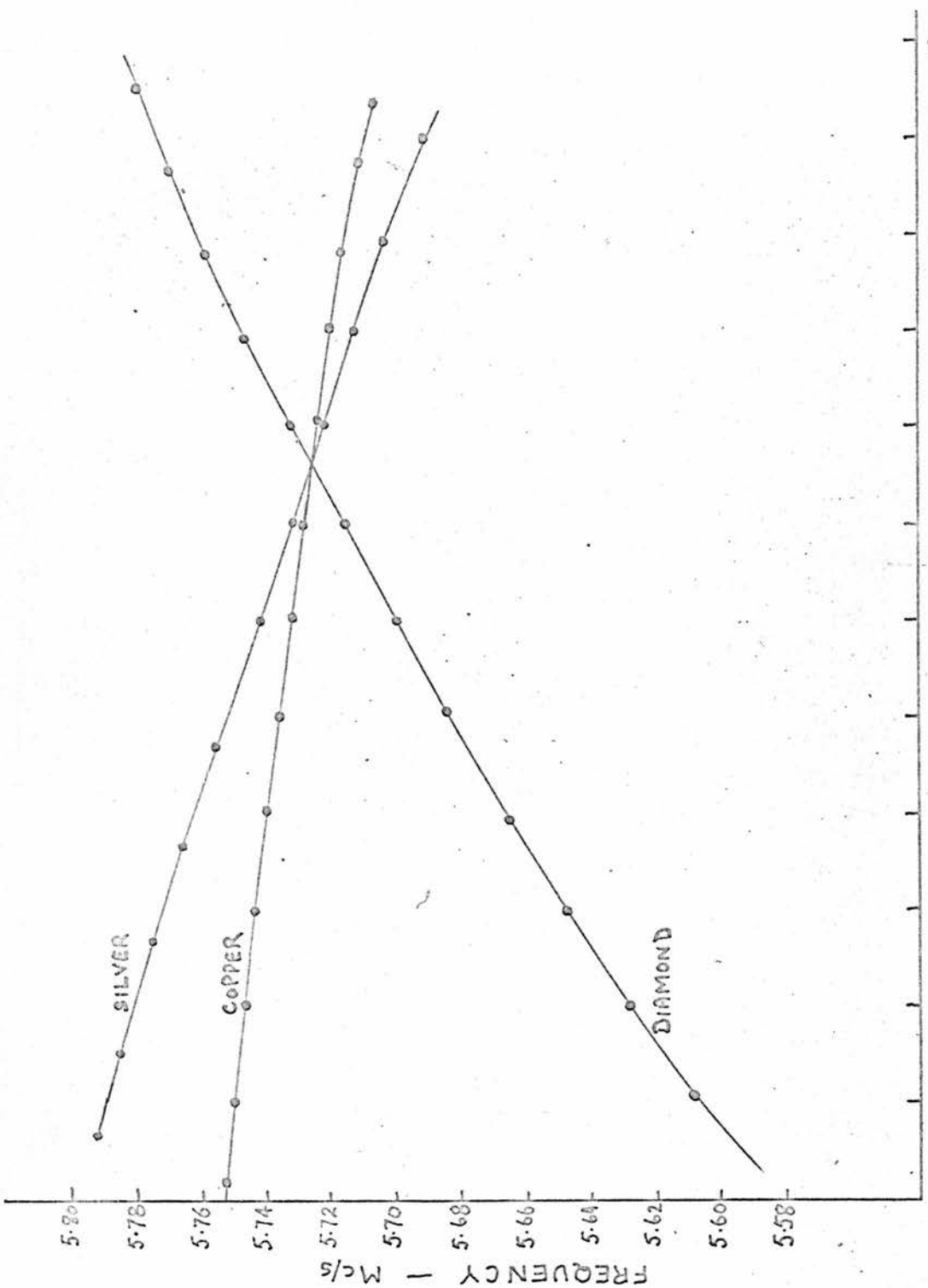

Figure 21 - Typical experimental results.

CHAPTER 5

RESULTS OF MEASUREMENTS

5.1 The method of calculating results.

The data as originally recorded were in the form of frequency readings and resistance thermometer readings. The resistances were converted to temperatures using the calibration values obtained at the ice point and at several points using the vapour pressure thermometer. Values of df/dx for the dilatometer were then calculated by assuming values of the linear thermal expansion coefficient for copper. The dilatometer gap was calculated as a function of temperature, for both the copper specimen and the diamond specimen. Referring to Fig.21 which shows the results of some of the experimental runs, one can see that at 21 5°K the copper and diamond runs intersect. At this point, since the frequencies are the same and the temperatures the same, one can assume that the dilatometer gap is the same for both cases; any spurious effect, if reproducible, will also be the same in both cases and it should be possible to calcul-

ate df/dx by starting at this point.

During preliminary experiments, two consecutive runs were made under very different conditions: one was made with a copper "mushroom" specimen[12] and the other with the membrane and normal copper specimen, the value of the dilatometer gap was also widely different in both cases. The df/dT values were similar for both runs but larger than values calculated by assuming the membrane and disc to be a parallel plate condenser. Because of the smallness of the dilatometer gap, there is a strong dependence of df/dT on the actual gap value and one would expect a large difference between the two df/dT values if they were caused mainly by the gap changes.

That this strong gap-dependence is not shown suggests that these large frequency changes are spurious although they are seen to be reproducible from the copper results and also from the reproducibility of later results. Consider Fig.22; theoretically df/dT for the copper specimen is positive but is seen here to be negative, so that if OB is the graph of frequency versus temperature for the copper specimen, then OA is the (f-T) graph expected if the gap does not change, the frequency change

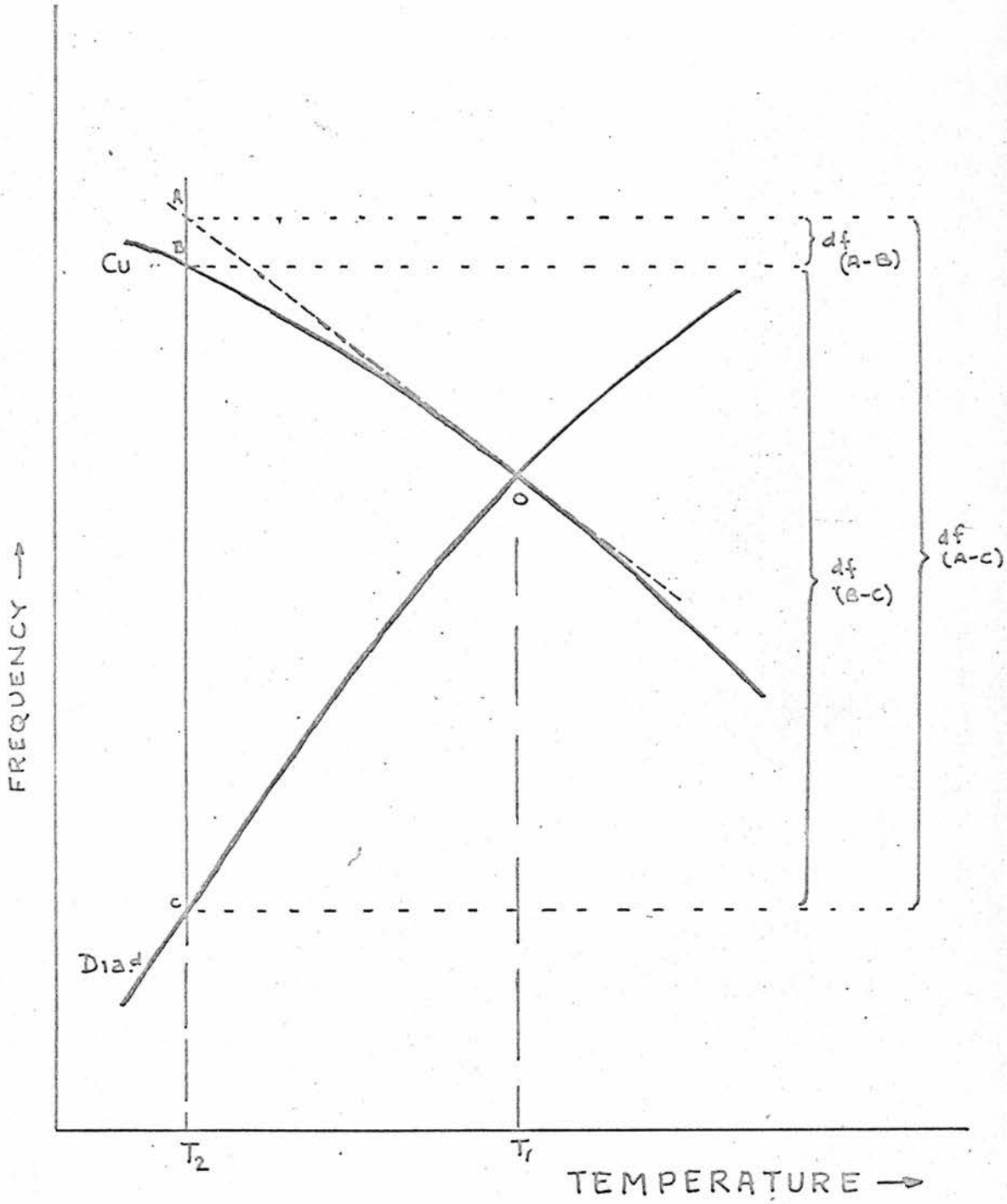

Figure 22 - Diagram of measured frequency changes.

being entirely spurious. Thus $df_{(A-B)}$ is the actual frequency change caused by the gap contracting during a temperature change from T_1 to T_2, and $df_{(A-C)}$ is the corresponding frequency change for the diamond specimen. Hence in going from temperature T_1 to T_2 the frequency change $df_{(B-C)}$ is caused by the difference in gap change between the diamond and copper cases, or

$$df_{(B-C)} \equiv dx_{(diamond)} - dx_{(copper)}$$

If the actual df values are measured from the frequency corresponding to the point 0, then the sum of the df values for copper and diamond runs will be the true frequency change caused by the difference in the change in the gap for the two cases. These frequency changes will provide the true df/dx values since the spurious effect has been eliminated, as has the change caused by expansion of the dilatometer top plate. df/dx values calculated on this basis are shown in Fig.20, where df/dx values are plotted against gap width and agree closely with the df/dx values measured by a micrometer.

To obtain the frequency changes for the copper and diamond runs, the values of df/dT were calculated and a smoothed curve drawn through the values: df/dT values

and df/dx values were thus obtained at 10°K intervals. Smoothed f against T curves were also drawn for the silver and aluminium runs.

Considering Taylor's expansion of the frequency as a function of x, the dilatometer gap, one can write

$$f(x_o + \Delta x) - f(x_o) = \Delta x \left(\frac{df}{dx}\right)_{x_o} + \frac{\Delta x^2}{2}\left(\frac{d^2f}{dx^2}\right)_{x_o}$$

where f(x) is the frequency at a gap value of x.

x_o is the gap value at some arbitrary temperature, in this case the temperature at which the two frequency-temperature curves intersect.

This can be written as

$$\Delta f = \left[\left(\frac{df}{dx}\right)_{x_o} + \frac{\Delta x}{2}\left(\frac{d^2f}{dx^2}\right)_{x_o}\right]\Delta x$$

and so

$$\Delta x = \frac{\Delta f}{\left(\frac{df}{dx}\right)_{x_o} + \frac{\Delta x}{2}\left(\frac{d^2f}{dx^2}\right)_{x_o}} .$$

Since $\left(\frac{d^2f}{dx^2}\right)_{x_o} \ll \left(\frac{df}{dx}\right)_{x_o}$ one can approximate Δx using

$$\Delta x = \frac{\Delta f}{\left(\frac{df}{dx}\right)_{x_o}}$$

Finally

$$\Delta x = \frac{\Delta f}{\left(\frac{df}{dx}\right)_{x_o} + \frac{\Delta f}{2}\left(\frac{d^2f}{dx^2}\right)_{x_o}\left(\frac{dx}{df}\right)_{x_o}} \qquad \ldots\ldots 5.1$$

Values of d^2f/dx^2 were obtained graphically by drawing tangents to the graph of df/dx against x. Putting measured values of Δf into equation 5.1 and using the calculated values of df/dx and d^2f/dx^2, values were obtained for Δx, the dilatation of the specimen relative to copper and hence the relative expansion coefficient. If the thermal expansion coefficient of copper is known, one can then find values for the expansion coefficient of the specimen. Corrections to Δf for the expansion of the top plate (P,Fig.7) and any spurious effects were obtained by subtracting the calculated Δf for a copper specimen from the measured Δf for copper; the remainder was assumed to be caused by changes other than the change in gap and is subtracted from the Δf of the unknown specimen.

Using the smoothed (f-T) values for the unknown

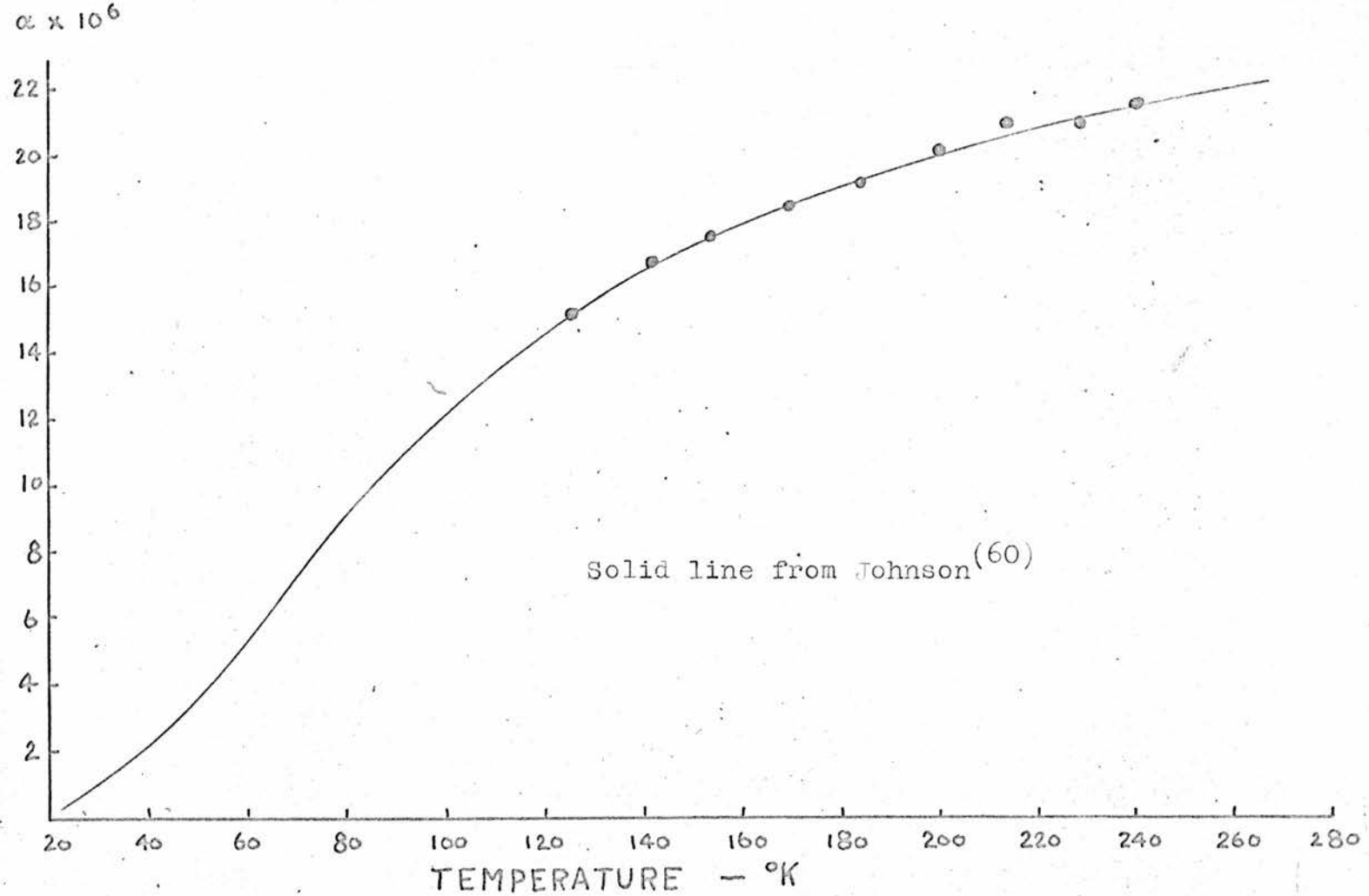

Figure 23 - Thermal expansion of aluminium.

specimen, the expansion coefficient was calculated at intervals of 10°K. Each calculated value was used to calculate the gap change and hence to find the df/dx value for the next calculation. Using these values a graph of the gap versus temperature was drawn and using this to determine the df/dx values the actual measured frequency changes were used to calculate the expansion coefficient, to obtain a more direct measurement. The values of the expansion coefficient for aluminium and silver are shown in Figs.23 and 24. In the only run made with an aluminium specimen, the gap was too large so that the frequency was too high. To give a further set of results which could be used to check the apparatus, the frequency changes were normalised to give a value of the expansion coefficient agreeing with the accepted value at 215°K.

5.2 Sensitivity and accuracy.

The resonant frequency of the circuit will be given by

$$4\pi^2 f^2 L(C+E) = 1 \qquad \ldots\ldots 5.2$$

where C is the specimen-controlled capacity, E is the stray capacity in the circuit (mainly that of the vib-

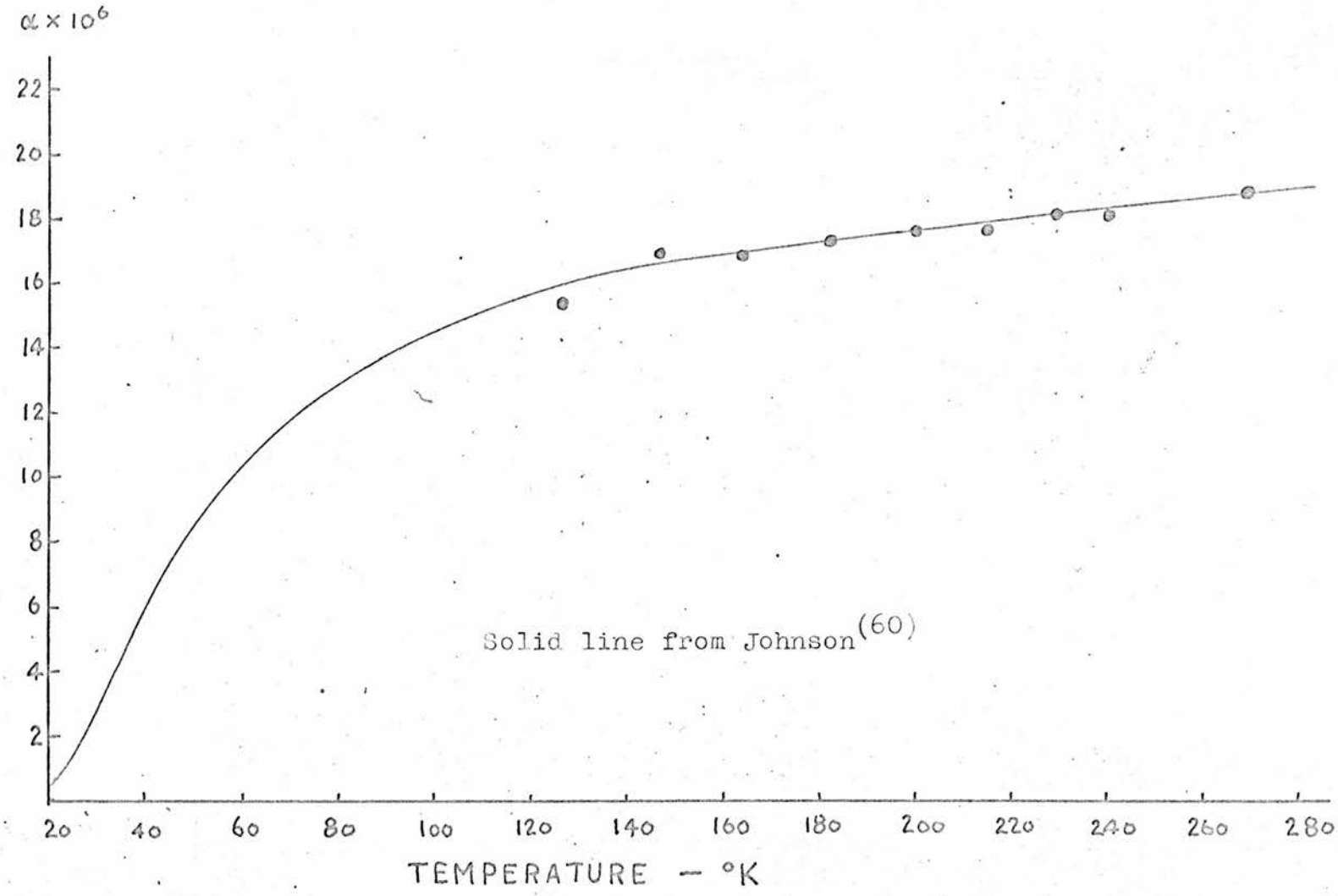

Figure 24 - Thermal expansion of silver.

rating reed condenser and the coaxial line down the centre of the cryostat), and L is the inductance of the coil. If E is assumed to be negligible (normally C/E > 15), and the dilatometer capacity assumed to be equivalent to a parallel plate condenser, it is easily shown that

$$\frac{df}{f} = \frac{dx}{2x} - \frac{dr}{r} \qquad \ldots 5.3$$

where x is the plate separation and r is the radius of the upper plate (P, Fig.7).

For copper, equation 5.3 reduces to

$$\frac{df}{f} = -\tfrac{1}{2}\alpha_{Cu}$$

where α_{Cu} is the coefficient of linear thermal expansion of copper.

For specimens of materials other than copper, equation 5.3 becomes

$$\frac{df}{f} = \frac{dx}{2x} - \alpha_{Cu}$$

Stewart has shown theoretically that f_o can be measured to within 1 c/s under ideal conditions[12]. The present apparatus however, does not achieve this accuracy. Even with extremely careful and meticulous 'setting up' procedures it was found impossible to obtain values of

the resonant frequency to better than $\pm$100c/s. A typical set of readings, taken with a copper specimen in the dilatometer is shown in Table 5.1 below.

Table 5.1

Time	f_0 (resonant frequency)
10.15	5,765,139
10.20	5,764,887 *
10.25	5,764,938 *
10.35	5,765,018 *
10.40	5,765,009
10.45	5,764,996

* low-frequency input to vibrating reed changed before next reading

From this it is seen that a small change (of the order of 1%) in the input frequency to the vibrating reed condenser can change the apparent resonant frequency of the resonant circuit by about 100c/s. To see why, consider C in equation 5.2 to be constant, then

$$\frac{df}{f} = - \frac{dE}{(C+E)}$$

If one allows a 1% change in the average value of the vibrating reed condenser (which is about 1pF) and considers C to be all the other capacities in the circuit (about 100pF), it is easily shown that the corresponding change in the resonant frequency is about 300c/s. It is therefore extremely important to use the vibrating reed condenser at a frequency well away from the reed resonance, so that the vibration amplitude is small and has as constant an amplitude as possible. Thus if the only error in measurement were in the measurement of the frequency change and if the frequency change were due entirely to a change in the length of the specimen (assuming dE to be zero), then from equation 5.3 the accuracy of measured length changes would be 1×10^{-7}cm.

The effect causing the dilatometer gap to change is the differential expansion between the specimen and the copper spacing ring in the dilatometer. For example, in the case of an aluminium specimen of length ℓ with a copper spacing ring, the relative length change will be $\ell \alpha \Delta T$ where α is the thermal expansion of aluminium relative to copper, about 5×10^{-6}per deg.K at 200°K. This will produce a gap change $dx = 1 \times 10^{-5}$cm per degree. If the accuracy of measurement is 1×10^{-7}cm, the final

accuracy in the measured expansion will be 0.1% for a ΔT = 10deg.K.

There are, however, frequency changes caused by effects other than changes in specimen length. These changes amount in some cases to a correction of up to 30% to be applied to the measured frequency change. Although a 3% error in the correction will give only 1% error in the final figure, it is desirable that these spurious (though reproducible) frequency changes should be reduced to a minimum. Allowing for the errors in the measurement of the spurious frequency change, the error in the final figure for the frequency change is probably less than 200c/s. With $df/dx = 0.8 \times 10^{8}$ c/s/cm and $dx = 1 \times 10^{-5}$ cm per deg.K, the error in the calculated figure would be 1.2% for a temperature change of 10deg.K. Since this estimation of accuracy is based on the df/dx values used in the calculation of the results, this order of accuracy is to be expected in the final results.

The spurious frequency changes seem to be caused by some peculiarity of the dilatometer itself, since all parts of the cryostat above the dilatometer were kept at a constant temperature (namely the boiling point of oxygen, which was the liquid in both the upper cans for

all the results obtained above). The only possible temperature variation outside the dilatometer itself is in the lead connecting the dilatometer to the coil, which passes from the dilatometer can via a glass-metal seal and through a central tube to the coil mounted on top of the cryostat.

During one experimental run, the liquid oxygen in the lower can was replaced by liquid nitrogen, keeping the dilatometer temperature constant; this changed the resonant frequency by 1kc/s. This change, although quite large, is caused by a temperature change of almost 13 degrees over a length of the central coaxial lead of at least 10cms where it passes through the lower can. At this portion of the central coaxial lead, the temperature change corresponding to a 10°C change in the dilatometer temperature must be considerably less than 10°C, while the frequency change correction is never less than 2kc/s. It is, however, possible that the temperature change of the top seal of the dilatometer could produce the observed frequency change; to check whether this was so, the glass-metal seal was replaced by a new seal but the alteration in the spurious frequency change was undetectable. The possibility that this glass-metal seal is the

cause of at least some of the spurious frequency changes is not completely ruled out, however, since the resonant circuit could be put off resonance by warming the region around this upper seal with a hair drier. Had time permitted, further attempts would have been desirable to trace the cause or causes of these spurious changes. However, since they were accurately reproducible, further investigation was postponed until evidence was available of the actual low temperature performance of the apparatus.

5.3 Results.

At low temperatures a sensitive representation of thermal expansion is provided by γ-T plots, where $\gamma(T)$ is defined by

$$\gamma(T) = \frac{\alpha V}{\chi_T C_v} = \frac{\alpha V}{\chi_s C_p}$$

and since C_p is the specific heat always measured, the $\gamma(T)$ used in the discussion of the results will be

$$\gamma(T) = \frac{\alpha V}{\chi_s C_p} \qquad \ldots . 5.4$$

The actual thermal expansion values calculated using the

TABLE 5.2

SILVER Θ = 225°K

T°K	T/Θ	ALPHA x 10^6	χ_S $cm^2 dyne^{-1}.10^{12}$	1/V $gm.at.cm^{-3}$	C_p erg/gm.at.degK.10^{-6}	GRUNEISEN	GAMMA
100	0.444	44.42	0.928	0.0983	20.17	2.414	2.37 (59)
120	0.533	46.62	0.932	0.0982	21.57	2.360	
140	0.623	48.60	0.935	0.0981	22.55	2.350	
150							2.38
160	0.711	50.31	0.939	0.0980	23.30	2.345	
180	0.800	51.72	0.942	0.0979	23.84	2.351	
200	0.880	52.89	0.946	0.0978	24.27	2.354	2.44
220	0.978	53.82	0.949	0.0977	24.60	2.359	
240	1.066	54.48	0.953	0.0976	24.92	2.350	
250							2.44
260	1.155	56.10	0.956	0.0975	25.24	2.380	
280	1.246	57.00	0.960	0.0974	25.35	2.400	
300	1.333	58.20	0.964	0.0973	25.46	2.439	2.38

ALUMINIUM Θ = 400°K

T°K	T/Θ	ALPHA x 10^6	χ_S $cm^2 dyne^{-1}.10^{12}$	1/V $gm.at.cm^{-3}$	C_p erg/gm.at.degK.10^{-6}	GRUNEISEN	GAMMA
100	0.250	38.0	1.150	0.10127	129.87	2.513	2.46 (59)
120	0.300	43.8	1.151	0.10116	156.60	2.402	
140	0.350	49.5	1.153	0.10107	176.58	2.405	
150							2.44
160	0.400	53.7	1.161	0.10096	192.51	2.380	
180	0.450	57.0	1.169	0.10085	205.20	2.358	
200	0.500	60.0	1.176	0.10073	215.19	2.353	2.44
220	0.550	62.4	1.185	0.10061	223.02	2.347	
240	0.600	64.5	1.193	0.10048	229.23	2.347	
250							2.38
260	0.650	66.3	1.203	0.10035	234.63	2.341	
280	0.700	----	1.213	0.10022	239.22	-----	
300	0.750	69.3	1.224	0.10008	243.54	2.322	2.34

(59) - Values from FRASER D.B. HALLETT A.C.H.

Reference 59.

procedure described in section 5.1 are shown in Figs.23 and 24, along with the values from the list of expansion coefficients compiled by Johnson[60] from a consideration of most of the measurements made up to the date of his compilation. In Table 5.2, values of α as measured are listed together with values of ρ, χ_s and C_p measured by other workers, followed by the values of $\gamma(T)$ calculated from equation 5.4.

For silver, the values of the Gruneisen $\gamma(T)$ are constant down to 120°K with deviations at both ends of the temperature range covered. It was noticed that the first reading of all the experimental runs deviated from the smooth curve expected; this was due to a delay in reaching thermal equilibrium in the dilatometer, after the relatively rapid heating to room temperature following the precooling of the dilatometer described in section 4.4. Apart from this first reading, the values of $\gamma(T)$ for silver are constant within 2.3% down to 120°K and agree well with values of $\gamma(T)$ reported by other workers: the last column in Table 5.2 gives the γ-values reported by Fraser and Hallett[59].

Gruneisen $\gamma(T)$ values derived for the aluminium specimen are also in close agreement with the values of

Fraser and Hallett. For aluminium, only one experimental run was made covering the temperature range from 100°K to room temperature. The results obtained for $\gamma(T)$ however, deviate by only 5% from the average value of 2.38, and are constant within 2.5% apart from the result at 100°K. There is some doubt about the accuracy of the value obtained at 100°K because the temperature of the dilatometer becomes more difficult to control as its temperature approaches that of the liquid coolant.

The thermal expansion coefficients obtained agree well with the values given by Johnson[60]. Table 5.3 lists the thermal expansion coefficient for silver obtained from a least squares fit to the experimental values measured. A polynomial was fitted to the points and values of the expansion coefficient calculated at 20°K intervals. The average deviation lies within the estimated 1.2% error limits.

5.4 Conclusions.

The results available for the expansion coefficients of silver and aluminium are in good agreement with those of other workers (Figs.23,24), showing that the method is satisfactory at least down to 100°K. The range may

be extended down to the limit imposed by the sensitivity of the detection system, using hydrogen and helium as refrigerants.

The Gruneisen γ-values for silver are constant down to 120°K but the γ-values for aluminium show a slight upward trend. The values of $\gamma(T)$ given by Fraser and Hallett have a spread of values which include all the values obtained from the present measurements: their results for aluminium also show an upward trend. This agreement gives confidence in the methods of measurement and calculation described above.

No special precautions were needed in mounting the cryostat, which was mounted on a frame fixed directly to the concrete floor of the laboratory. The apparatus was stable against reasonable vibration in the laboratory. Specimen preparation and changing is easily carried out. Temperature stability was very good indeed because of the large heat capacity of the dilatometer and temperature control was very easy.

The apparatus would be improved by incorporating a secondary calibration method so that a mechanical calibration could be made at low temperatures. An adaptation of the system used by Andres[14] would be possible as

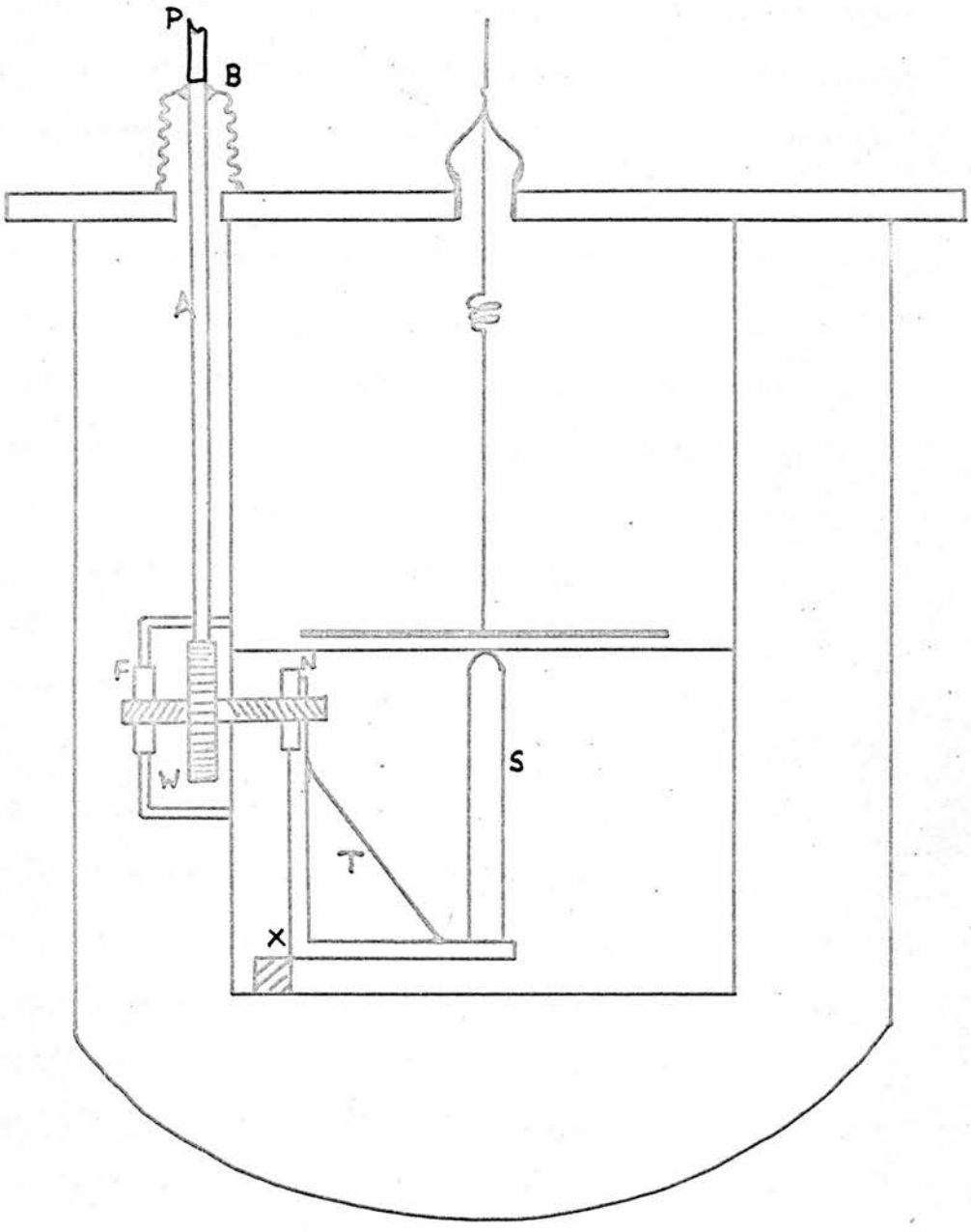

Figure 25 - Proposed calibration device.

shown in Fig.25. A push-rod A, carrying a ratchet causes the toothed wheel W to revolve turning an axle carrying two nuts: F is fixed and has a thread of opposite direction to that of N. The triangular structure T can thus be rotated around the fixed point X, moving the specimen S in a vertical direction. The push-rod A is soldered to a length of copper bellows B which can be compressed using the rod P which passes down from the head of the cryostat and may be withdrawn from contact with B to reduce the heat leak at lower temperatures.

Further work is necessary to remove or minimise the spurious frequency changes described in section 5.2 before extension of the measurement to lower temperatures. The possibility of heating the sample only and keeping the dilatometer temperature fixed is worth considering. If the spurious frequency changes are due to the strains induced in the top plate of the dilatometer, they would then be eliminated. Dispensing with the vibrating reed condenser would remove one source of error, which may be quite large, as shown in section 5.2. The commercial availability of signal generators such as the Schlumberger type DO 1001 frequency synthesiser makes this now possible. This can supply a frequency modulated

output in the 1 - 50Mc/s range with a centre frequency short term stability of 2 parts in 10^8. Using apparatus of this kind would make it possible to dispense with the vibrating reed condenser.

Table 5.3

Expansion coefficient for silver.

$T^{o}K$	β^{*}	$\alpha = 3\beta$	Present Result	Deviation %
100	14.6	43.8	44.4	+1.3
120	15.8	47.4	46.6	-1.7
140	16.5	49.5	48.6	-2.0
160	16.9	50.7	50.3	-0.8
180	17.3	51.9	51.7	-0.4
200	17.7	53.1	52.9	-0.4
220	18.1	54.3	53.8	-0.9
240	18.5	55.5	54.5	-1.8
260	18.8	56.4	56.1	-0.5
280	19.0	57.0	57.0	0
300	19.3	57.9	58.2	+0.5

* - value from Johnson[60]

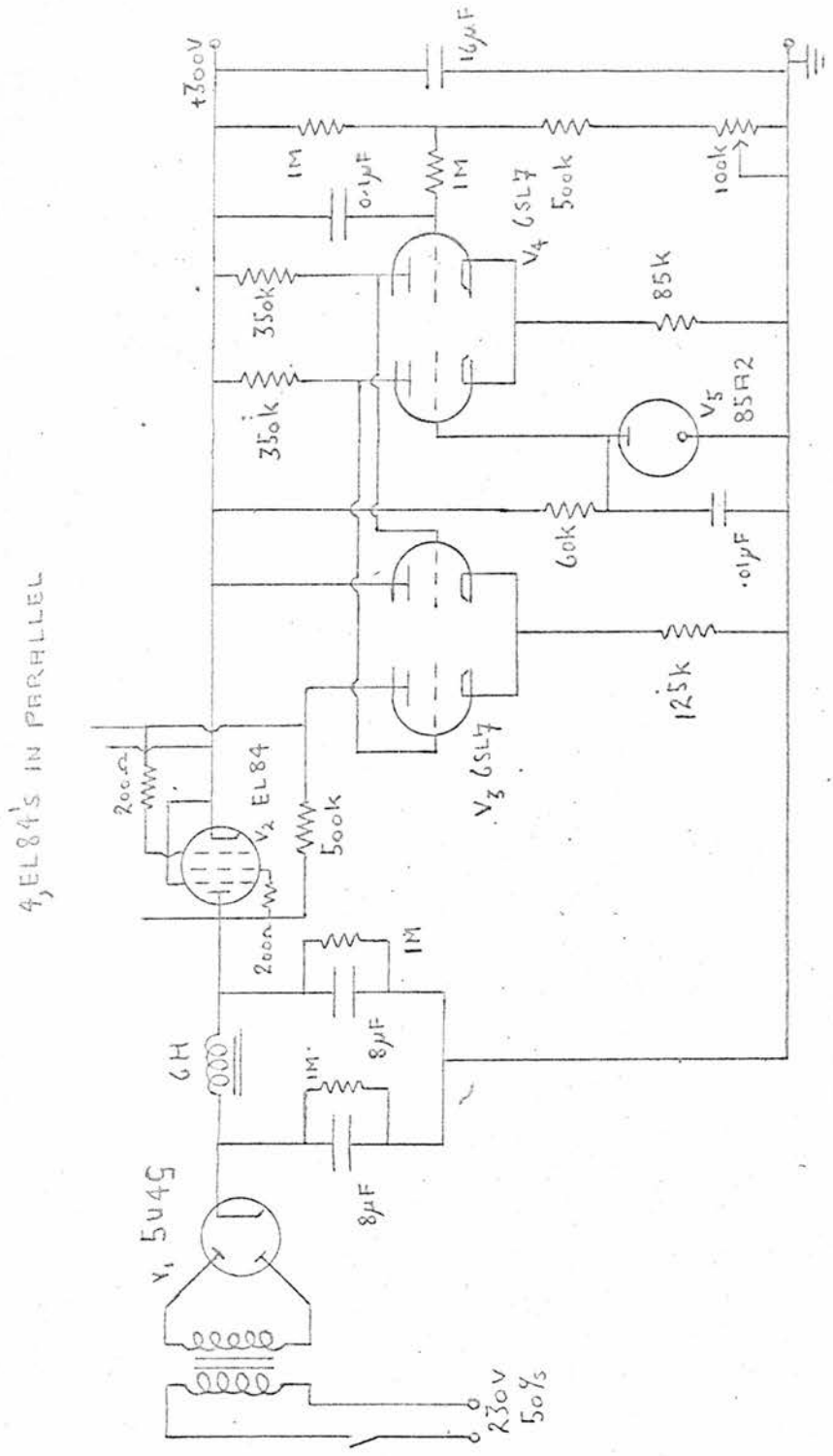

Figure 26 - Power pack No.1.

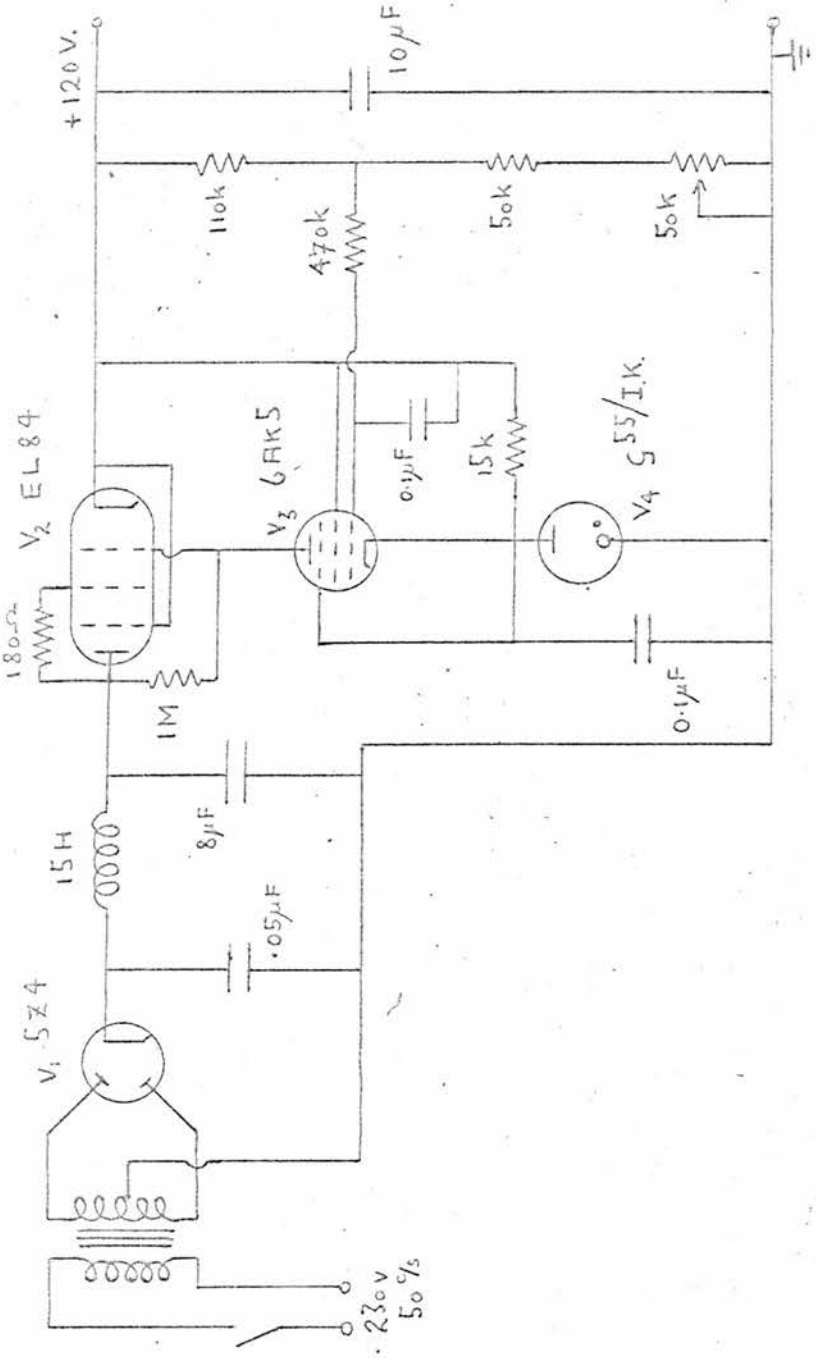

Figure 27 - Power pack No.2.

Figure 6 - Photograph of the cryostat.

REFERENCES

1. Bijl D., Prog. in Low Temp. Physics. Vol.2. (1955)
2. Furth R., Proc.Roy.Soc. A183, p.87(1945)
3. Mie G., Ann.d.Phys. 11, p.657(1903)
4. Gruneisen E., Hndbch.d.Phys. 10, p.1(1926)
5. Gruneisen E., Ann.d.Phys. 26, p.211(1908)
6. Barron T.H.K., Phil.Mag. 46, p.720(1955)
7. Bijl D., Pullan H., Phil.Mag. 45, p.290(1954)
8. Debye P., Ann.d.Phys. 39, p.789(1912)
9. Simmons R.O., Baluffi R.W., Phys.Rev. 108, p.278(1957)
10. Prytherch W.E., J.Sci.Inst. 9, p.128(1932)
11. Pullan H., Thesis. Oxford(1953) unpublished.
12. Stewart T.B., Thesis. St Andrews(1962) unpublished.
13. Huzan E., Abbiss C.P., Jones G.O., Phil.Mag. 6, p.277(1961)
14. Andres K., Cryogenics. 2, p.93(1961)
15. Jones R.V., J.Sci.Instr. 28, p.38(1951)
16. Andres K., Helv.Phys.Acta. 34, p.398(1961)
17. White G.K., Cryogenics. 1, p.151(1961)
18. White G.K., Nature. 187, p.827(1960)
19. White G.K., Phil.Mag. 6, p.815(1961)
20. White G.K., Aust.J.Phys. 14, p.359(1961)
21. Dheer P.N., Surange S.L., Phil.Mag. 3, p.665(1958)

22. Einstein A., Ann.d.Phys. 22, p.180, p.800(1907)
Ann.d.Phys. 34, p.170, p.590(1911)
23. Einstein A., Ann.d.Phys. 35, p.679(1912)
24. Born M., von Karman T., Phys.Zeits. 13, p.297(1912)
25. Born M., Goeppert-Mayer M., Enc.d.Phys. 24/2, (1933)
26. Blackman M., Enc.d.Phys. 7/1, p.340(1955)
27. Born M., Atomtheorie des Festen Zustandes
(1923) Leipzig.
28. Blackman M., Proc.Roy.Soc. A159, p.416(1937)
29. Fine P.C., Phys.Rev. 55, p.355(1939)
30. Kellerman E.W., Proc.Roy.Soc. A178, p.17(1941)
31. Montroll E.W., J.Chem.Phys. 10, p.218(1942)
32. Leighton R.B., Rev.Mod.Phys. 20, p.165(1948)
33. Furth R., Proc.Camb.Phil.Soc. 37, p.34(1941)
34. Bradburn M., Proc.Camb.Phil.Soc. 39, p.113(1943)
35. Gow M.M., Proc.Camb.Phil.Soc. 40, p.151(1944)
36. Bijl D., Pullan H., Physica 21, p.295(1955)
37. Seitz F., Modern Theory of Solids, New York, (1940)
38. Klein M.J., Glass S.J., Phil.Mag. 3, p.538(1958)
39. Blackman M., Proc.Phys.Soc. B70, p.827(1959)
40. Blackman M., Phil.Mag. 3, p.831(1958)
41. Novikova S.I., Fiz. tverdogo Tela. 2, p.43(1960)
42. Novikova S.I., Fiz. tverdogo Tela. 2, p.1617(1960)

43. Gibbons D.F., Phys.Rev. 112, p.136(1958)

44. Blackman M., Proc.Phys.Soc. B74, p.17(1959)

45. Horton G.K., Can.J.Phys. 39, p.263(1961)

46. Nix F.C., McNair D., Phys.Rev. 60, p.597(1941)
Phys.Rev. 61, p.74(1942)

47. Slater J.C., Introduction to Chemical Physics.
New York, (1941)

48. Barron T.H.K., Annals of Phys. 1, p.77(1957)

49. Daniels W.B., Phys.Rev.Letters. 8, p.3(1962)

50. de Launey J., Solid State Physics. 2, p.233(1956)

51. Villard N., Rev.Sci.Inst. 22, p.726(1951)

52. Schuster N.A., Rev.Sci.Inst. 22, p.254(1951)

53. Dobbs E.R., Jones G.O., Repts.Prog.Phys. 20,
p.516(1957)

54. Gibbons D.F., J.Phys.Chem.Solids. 11, p.246(1959)

55. Leibfried G., Ludwig W., S.State.Physics. 12,
p.275(1961)

56. Collins J.G., Phil.Mag. 8, p.323(1963)

57. Born M., Proc.Camb.Phil.Soc. 39, p.100(1943)

58. Barron T.H.K., Klein M.L., Phys.Rev. 127,
p.1997(1962)

59. Fraser D.B., Hallett A.C.H., Proc.7th.Int.Conf. on
Low Temp. Physics. p.689 Toronto, (1960)

60. Johnson V.J., Properties of Materials at Low Temperature. Pergamon Press. (1961)

ACKNOWLEDGEMENTS

I should like to thank the following for all the help I received and record my debt to :-

Professor J.F.Allen, F.R.S.	- for allowing me the facilities of Edgecliffe Research Laboratory.
Dr D.Bijl, F.R.S.E.	- for his advice and supervision.
Mr J.Gerrard	- for the photography.
Mr R.Mitchell	- for supplying the liquid coolants and much valuable advice.
Messers J.McNab, M.Bird, G.Dunsire and F.Akerboom.	- for help in construction of apparatus.
Mr T.B.Stewart, M.Sc.	- without whose help this thesis could not have been written.
My Father	- for help at all times.
My Wife	- for her patience and understanding and efficient typing of the thesis.